Neutron Resonance Spectroscopy. VI. Mo, Sb, Te, and Pr†

S. WYNCHANK, J. B. GARG,* W. W. HAVENS, JR., AND J. RAINWATER
Columbia University, New York, New York
(Received 2 October 1967)

The total neutron cross sections of natural Mo, Te, Sb, and Pr have been measured from about 6 eV to a maximum energy of 250 keV for Mo and Pr and to about 5 keV for Sb and Te, using the Nevis synchrocyclotron and a 200-m flight path. The maximum time resolution is 0.5 nsec/m. The resonance energies and the neutron reduced widths of about 1000 levels have been obtained, using area analysis. Values of $\Gamma_\gamma \sim 100$ meV were obtained for the capture widths of 15 levels in natural Sb. Values of the spin J of the compound nucleus were obtained for a number of levels of Pr. Our values for the s-wave strength function for Mo, Sb, Te, and Pr are $S_0 = (0.35 \pm 0.06)$, (0.34 ± 0.05), (0.15 ± 0.03), and $(1.72 \pm 0.25) \times 10^{-4}$, respectively. An average level spacing $\langle D \rangle = 75.2$ eV was obtained for Pr. The presence of many p-wave levels led to a strong energy dependence of the observed $\langle D \rangle$ for Mo, Sb, and Te. The observed statistical distributions of the neutron reduced widths and nearest-neighbor level spacings for Pr and natural Sb are compared with the Porter-Thomas and Wigner distributions, respectively.

I. INTRODUCTION

THIS is the sixth in a series[1] of papers reporting the results of neutron time-of-flight cross-section studies using the Columbia University synchrocyclotron. Total-cross-section (transmission) measurements were made using 0.5-nsec/m maximum resolution and several transmission sample thicknesses for each of the natural elements: Mo [$Z=42$; $A=92(0.164)$, $94(0.093)$, $95(0.158)$, $96(0.165)$, $97(0.094)$, $98(0.223)$, $100(0.087)$], Sb [$Z=51$; $A=121(0.576)$, $123(0.424)$], Te [$Z=52$; $A=120(0.0010)$, $122(0.026)$, $123(0.009)$, $124(0.047)$, $125(0.071)$, $126(0.189)$, $128(0.317)$, $130(0.339)$], Pr [$Z=59$; $A=141(1.00)$]. The quantity in brackets for each isotope is the fraction of the atoms of the element due to the particular isotope.

The energy range studied was from ~ 6 eV to >100 keV. The useful upper limit where most resonances were resolved was much lower and element-dependent. The measurements fill a gap in a region of A values previously recorded. The region $A=90$ to 130 is a region of a relative maximum for the p-wave ($l=1$) strength function S_1, and a minimum for the s-wave ($l=0$) strength function S_0. Praseodymium, with $A=141$, is near the beginning of a region of maxima for S_0 for deformed nuclei, but Pr^{141} has closed-shell neutron number $N=82$ and relatively spherical shape. The observation of an excess of weak levels for all four elements presumably reflects the presence of many relatively strong $l=1$ levels. This interpretation is less certain for Pr.

For all but Pr, the isotope identification of the individual observed resonances is not known except for some of the lower-energy resonances where poorer resolution measurements have been made by other investigators using separated isotopes. We list the level energy E_0 and the "strength" parameters ($ag\Gamma_n^0$) for each of several hundred analyzed resonances, where a is the fractional abundance of the responsible isotope (as listed above), g is the usual spin weight factor, and Γ_n^0 is the reduced neutron level width $\Gamma_n(1eV/E_0)^{1/2}$. In some favorable cases we also obtain the total level width Γ, the capture width Γ_γ, or the favored value of the spin J of the compound nucleus. The strength functions S_0 are evaluated and the statistical distributions of parameters are analyzed and compared with theories where appropriate.

II. EXPERIMENTAL DETAILS AND LEVEL PARAMETER ANALYSIS

The main experimental arrangements of the system used in these measurements have been described earlier.[2] The principal new aspects are as follows:

(1) The 12-×48-in. B^{10} slab at the 200-m station is now viewed by four large γ-ray detectors, each having a NaI volume, 11 in. in diameter by 2 in. thick, viewed by a 5-in.-diam photomultiplier. Their use has approximately doubled the efficiency of detection of the γ rays from the neutron capture reaction $B^{10}(n,\alpha)Li^{7*}$.

(2) A 37-m detector station was used at the lowest energies (≥ 6 eV). This used an aperture of $\sim 2\frac{1}{2} \times 11$ in., with a B^{10} slab viewed above and below by large plastic scintillator γ detectors. The station has also been used for self-indication measurements for other elements.

(3) The path in air has been further reduced by the use of helium-filled balloons in the main cyclotron shielding wall (between the neutron source and the

† Work supported in part by the U. S. Atomic Energy Commission.

* National Science Foundation Grant. Present address: State University of New York at Albany, Physics Department, Albany, N. Y.

[1] Earlier papers in this series: I: J. L. Rosen, J. S. Desjardins, J. Rainwater, and W. W. Havens, Jr., Phys. Rev. **118**, 687 (1960), U^{238}. II: J. S. Desjardins, J. L. Rosen, W. W. Havens, Jr., and J. Rainwater, *ibid.* **120**, 2214 (1960), Ag, Au, Ta. III: J. B. Garg, J. Rainwater, J. S. Petersen, and W. W. Havens, Jr., *ibid.* **134**, B985 (1964), Th^{232}, U^{238}. IV: J. B. Garg, W. W. Havens, Jr., and J. Rainwater, *ibid.* **136**, B177 (1964), As, Br. V: J. B. Garg, J. Rainwater, and W. W. Havens, Jr., *ibid.* **137**, B547 (1965), Nb, Ag, I, Cs.

[2] J. Rainwater, W. W. Havens, Jr., and J. B. Garg, Rev. Sci. Instr. **35**, 263 (1964).

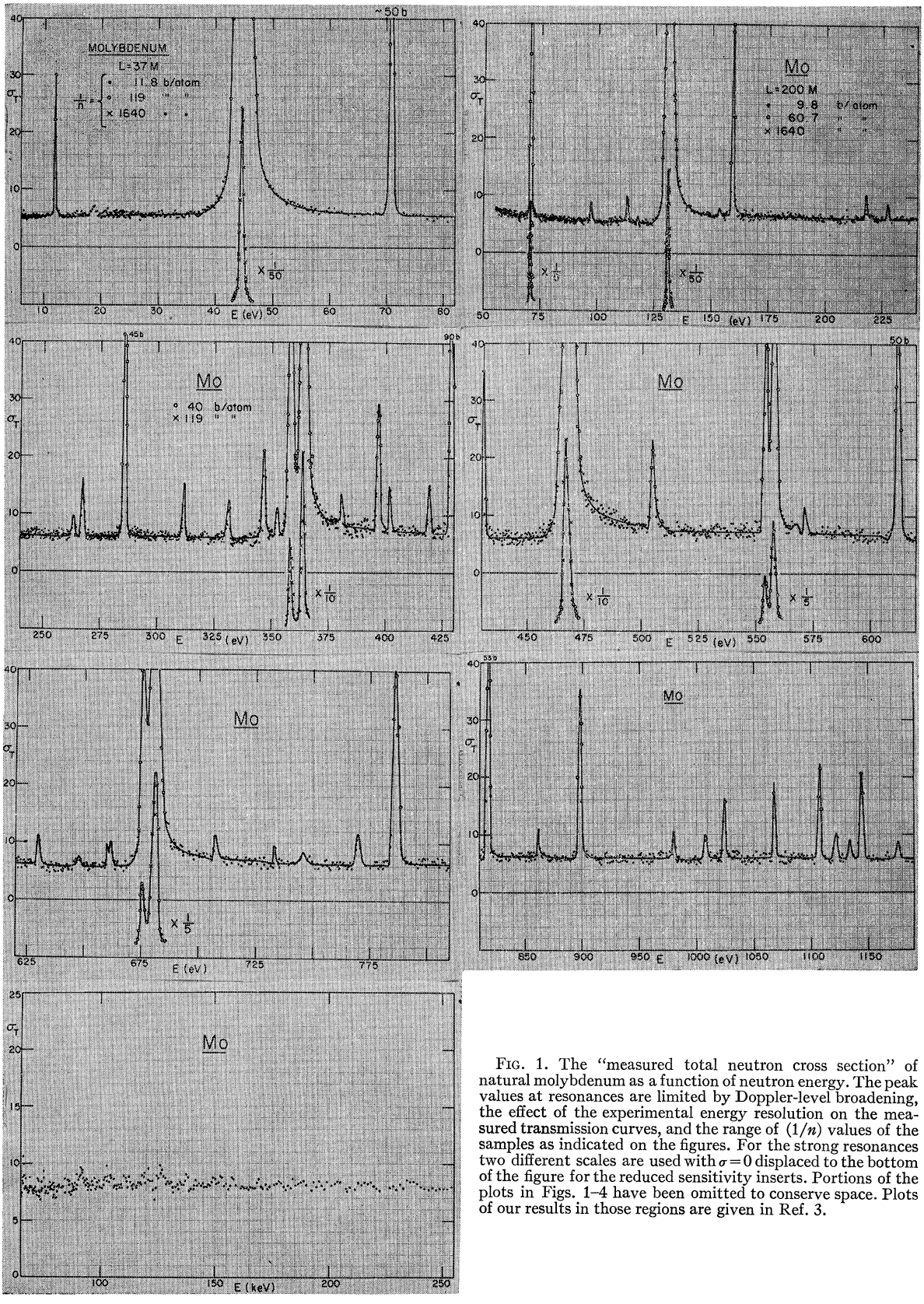

FIG. 1. The "measured total neutron cross section" of natural molybdenum as a function of neutron energy. The peak values at resonances are limited by Doppler-level broadening, the effect of the experimental energy resolution on the measured transmission curves, and the range of $(1/n)$ values of the samples as indicated on the figures. For the strong resonances two different scales are used with $\sigma=0$ displaced to the bottom of the figure for the reduced sensitivity inserts. Portions of the plots in Figs. 1–4 have been omitted to conserve space. Plots of our results in those regions are given in Ref. 3.

TABLE I. The energies E_0 and values of $ag\Gamma_n^0$ for resonances in natural Mo. The letters A, B, ···, G show isotope assignments for $A=92$, 94, 95, 96, 97, 98, and 100 based on the work of Pevsner *et al.*[a] For Mo, Sb, Te, and Pr, we have E_0, but not $ag\Gamma_n^0$ values for a range of energy above those shown in Tables I–V. These resonance energies are listed in another report.[b]

	E_0 (eV)	ΔE_0 (eV)	$ag\Gamma_n^0$ (meV)	$\Delta ag\Gamma_n^0$ (meV)
E	70.93	0.03	0.14	0.02
G	97.34	0.06	0.004	0.001
D	113.44	0.07	0.004	0.001
C	117.73	0.07	0.001	0.001
D	131.40	0.08	4.7	0.4
	154.72	0.05	0.001	0.001
C	159.46	0.06	0.08	0.01
C	217.86	0.09	0.007	0.002
E	227.31	0.10	0.005	0.001
C	263.71	0.12	0.005	0.002
E	268.11	0.12	0.04	0.01
E	285.88	0.14	0.16	0.02
E	311.87	0.15	0.028	0.004
C	331.44	0.17	0.022	0.008
A	346.82	0.18	0.06	0.02
	352.36	0.18	0.03	0.01
C	358.23	0.19	1.4	0.4
G	363.67	0.19	2.6	0.7
	380.56	0.20	0.03	0.01
E	396.92	0.22	0.11	0.04
	401.72	0.22	0.043	0.006
	419.00	0.24	0.027	0.005
F	429.04	0.25	0.62	0.05
F	467.16	0.28	4.5	0.7
F	504.96	0.30	0.11	0.01
C	553.91	0.35	0.40	0.10
E	557.85	0.35	1.2	0.1
	566.98	0.35	0.02	0.01
	571.50	0.40	0.04	0.01
F	612.40	0.40	0.35	0.06
	629.76	0.45	0.05	0.02
	647.88	0.45	0.04	0.02
	661.00	0.45	0.06	0.01
	675.83	0.50	0.70	0.40
C	681.15	0.50	2.5	0.9
E	707.17	0.50	0.08	0.01
	733.08	0.55	0.06	0.01
	745.18	0.55	0.08	0.02
C	769.71	0.60	0.09	0.02
E	786.34	0.60	0.65	0.20
F	818.05	0.65	1.8	0.3
	862.70	0.70	0.07	0.05
C	899.18	0.75	0.62	0.08
	981.14	0.85	0.07	0.02
	1008.62	0.90	0.10	0.02
C	1025.48	0.90	0.18	0.07
G	1069.06	0.95	0.21	0.04
F	1108.38	1.00	0.40	0.05
	1122.66	1.05	0.12	0.06
	1135.12	1.05	0.05	0.02
C	1144.59	1.05	0.37	0.08
	1177.06	1.10	0.09	0.02
	1204.00	1.15	0.30	0.02
G	1251.00	1.20	0.72	0.25
E	1260.80	1.25	0.29	0.08
	1270.70	1.25	0.05	0.02
	1319.00	1.30	0.07	0.02
	1341.70	1.35	0.10	0.05
	1364.90	0.70	0.05	0.02
	1404.40	0.70	0.15	0.05
C	1418.90	0.75	0.42	0.08
	1425.50	0.75	0.06	0.02
	1495.70	0.80	0.17	0.07
	1497.30	0.80	0.36	0.08
F	1526.30	0.80	2.4	0.4
	1535.30	0.80	0.50	0.20
	1541.90	0.85	1.8	0.8
	1590.20	0.85	0.57	0.19
	1597.20	0.90	0.21	0.08
	1679.00	0.95	0.14	0.05
B	1697.00	0.95	0.62	0.17
	1714.00	0.95	0.24	0.08
	1767.90	1.00	0.77	0.09
	1867.50	1.10	0.02	0.01
	1871.90	1.10	0.02	0.01
	1921.70	1.15	0.02	0.01
	1937.90	1.15	0.75	0.30
B	1950.80	1.20	0.70	0.20
	2027.30	1.20	0.02	0.01
	2044.90	1.25	0.43	0.18
	2051.20	1.25	0.40	0.15
	2062.70	1.30	0.01	0.01
	2088.60	1.30	0.37	0.10
	2116.30	1.35	0.15	0.05
	2132.40	1.35	0.49	0.11
	2143.20	1.35	0.10	0.03
	2152.70	1.35	0.10	0.05
	2166.50	1.40	0.20	0.05
	2177.50	1.40	0.74	0.26
	2299.20	1.50	0.14	0.05
	2322.00	1.55	0.23	0.10
D	2363.90	1.60	13.0	1.0
	2421.60	1.65	0.80	0.30
	2438.00	1.65	0.28	0.10
	2462.90	1.65	0.56	0.20
	2484.80	1.70	0.20	0.08
	2496.70	1.70	0.06	0.04
	2532.95	1.75	0.08	0.04
F	2550.40	1.75	2.2	0.7
	2580.70	1.80	0.80	0.30
	2602.30	1.80	0.14	0.04
	2615.00	1.85	0.16	0.04
	2633.50	1.85	0.40	0.20
	2697.00	1.90	0.14	0.06
	2730.05	1.95	0.11	0.05
	2760.00	2.00	0.15	0.06
	2779.90	2.00	0.40	0.20
	2843.20	2.00	0.15	0.10
	2868.20	2.00	0.08	0.05
	2947.60	2.00	0.10	0.05
	3007.6	2.0	1.55	0.45
	3041.0	2.0	0.33	0.10
	3062.0	2.0	0.27	0.10
	3074.0	2.0	0.25	0.08
	3119.0	2.5	0.15	0.10
	3128.0	2.5	0.19	0.08
A	3169.6	2.5	30.	10
	3209.0	2.5	0.25	0.09
	3219.0	2.5	0.05	0.05
	3264.0	2.5	0.56	0.20
D	3282.0	2.5	24	10
F	3292.8	2.5	20	10
	3339.8	2.5	0.28	0.10
	3369.0	3.0	0.19	0.07
	3392.0	3.0	0.38	0.15
	3489.9	3.0	0.35	0.15
	3504.0	3.0	0.57	0.20
	3573.0	3.0	9.5	2.0
	3599.0	3.0	1.7	1.0
	3623.0	3.0	0.60	0.20
	3644.0	3.0	0.05	0.05
	3650.5	3.0	0.50	0.10
	3671.7	3.0	0.10	0.10
	3696.0	3.0	0.10	0.10
	3726.0	3.0	1.38	0.40
	3758.0	3.0	1.0	0.4
	3799.8	3.0	1.2	0.6
	3832.0	3.5	0.10	0.10
	3845.0	3.5	0.05	0.05
	3868.0	3.5	0.08	0.05

[a] Reference 4. [b] Reference 3.

TABLE I (*continued*)

E_0 (eV)	ΔE_0 (eV)	$ag\Gamma_n^0$ (meV)	$\Delta ag\Gamma_n^0$ (meV)	E_0 (eV)	ΔE_0 (eV)	$ag\Gamma_n^0$ (meV)	$\Delta ag\Gamma_n^0$ (meV)
3881.0	3.5	0.10	0.08	4401.0	4	0.40	0.20
4013	4	0.83	0.20	4482	5	1.1	0.5
4034	4	0.37	0.20	4507	5	0.30	0.10
4062	4	0.20	0.10	4515	5	0.25	0.10
4088	4	0.10	0.10	4557	5	0.04	0.04
4127	4	0.10	0.10	4574	5	1.9	0.7
4138	4	0.53	0.15	4616	5	0.70	0.10
4178	4	0.34	0.10	4673	5		
4193	4	0.01	0.10	4708	5	0.36	0.20
4215	4	0.23	0.10	4726	5	0.28	0.15
4287	4	1.2	0.3	4739	5	0.25	0.10
4322	4	0.84	0.30	4843	5	3.5	1.0
4342	4	0.03	0.03	4930	5	1.4	0.4
4361	4	0.70	0.20	5043	5	0.21	0.10
4389	4	0.40	0.20				

transmission sample) and at the 35-m house. This should have increased the intensity by $\sim 20\%$.

The data were analyzed using IBM types 1620 and 7094 computers. Resonance parameters were obtained using an area analysis of the transmission dips, the details of which have been given previously.[1] The analysis is based on the Breit-Wigner single-level formula and includes interference between potential and resonance scattering and Doppler-level broadening effects.

A. Molybdenum

The neutron transmission measurements for natural molybdenum were made in six different energy regions: (1) 5–80 eV, (2) 50–150 eV; (3) 150–350 eV; (4) 300–1200 eV; (5) 1200 eV–5 keV; and (6) 4–250 keV. The lowest-energy region (1) used a flight path of 37 m and a channel width of 0.4 μsec. All other energy-interval measurements were made using a flight path of 200 m with detection channel widths of 0.4, 0.2, 0.2, 0.1, and 0.1 μsec, respectively. Different sample thicknesses having $1/n=9.9$, 11.8, 40, 60.7, 119, and 1640 b/atom were used for these measurements; the thinnest sample ($1/n=1640$) was used for the lowest-energy region only. The curves of "measured" σ_T versus neutron energy for natural Mo are shown in Fig. 1, and the values of the resonance parameters are given in Table I. Only portions of our curves of "measured" σ_T versus neutron energy for Mo are shown in Fig. 1, since the curves showing our results in the energy regions not shown in Fig. 1 are contained in a recently issued neutron cross section compilation volume.[3] The same remark applies to Figs. 2–4 for Sb, Te, and Pr. The final values of the level parameters, as given in Tables I–V, differ in many cases from our preliminary values listed in Ref. 3.

In viewing plots, such as Figs. 1–4, it should be noted that these are not intended to imply the true form of σ versus E at the resonances even when Doppler-level broadening effects are included. The $(1/n)$ values of the samples have the units of cross section (b/atom). The measured transmission value for any channel, $\exp(-n\sigma)$, has as its exponent the ratio of some suitable "transmission average" of σ for the channel to the sample $(1/n)$ cross section. The "measured σ" for any channel can never be more than a few times $(1/n)$, and will be unreliable if σ is very small compared with $(1/n)$. Thus the indicated "measured σ" may be much reduced from the true σ at exact resonance. The derived level parameters of the tables should be used to calculate a more meaningful shape for σ versus E for any critical applications. In particular, while the "area" of the observed resonance transmission dip is not influenced by the instrumental energy resolution, the "area" of the measured σ versus E peak is usually much less than for the true σ versus E peak. The utility of the plots is: (a) the display of σ between levels, (b) the positions of the levels, (c) the relative degree of experimental resolution and the certainty of identification of levels, and (d) a qualitative indication of the strength of each resonance relative to neighboring levels.

Since our measurements do not identify the isotope responsible for each level, we obtain the level "strength" parameter in the form $ag\Gamma_n^0$. The tables indicate the isotope identifications for those resonances which have been identified by other investigators using separated isotope samples.

B. Antimony

The total-cross-section measurements on natural antimony were made using energy intervals of (1) 5–80 eV; (2) 50–150 eV; (3) 150–350 eV; (4) 300–1200 eV; (5) 1200–5000 eV; with a flight path of 37 m for the lowest-energy region (1) and 200 m for all the other regions. The channel widths of the time analyzer were 0.4 μsec at 37 m; and 0.4, 0.2, 0.2, and 0.1 μsec, respectively, for other regions. The samples used had thicknesses corresponding to $1/n=11.5$, 50, and 400 b/atom for region (1); $1/n=7.92$, 31.1, 112, and 400

[3] Brookhaven National Laboratory Report No. BNL 325 (U. S. Government Printing Office, Washington, D. C., 1966), 2nd ed., Suppl. 2, Vol. IIB.

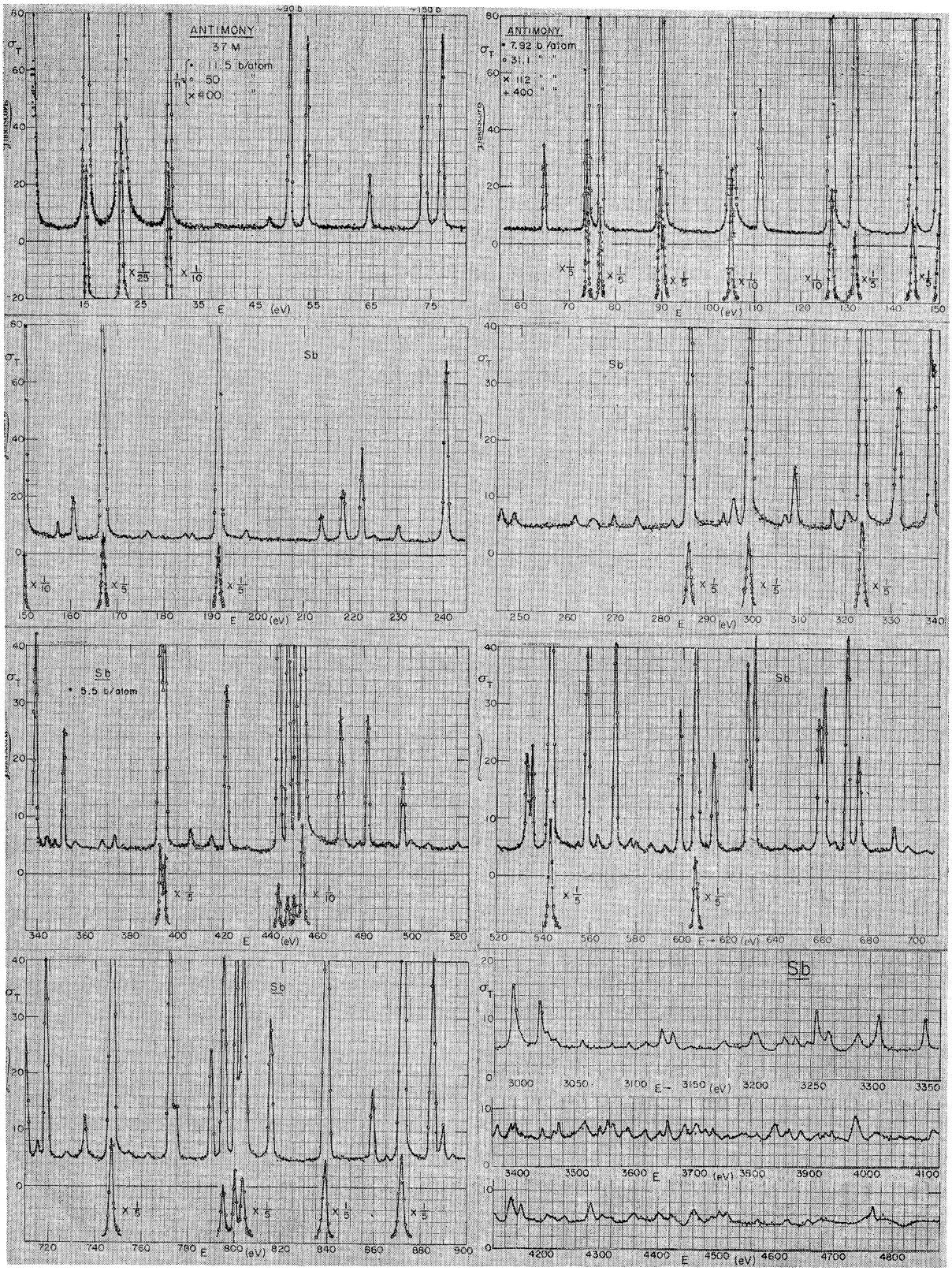

FIG. 2. The "measured" σ_T-versus-E_n curves for natural antimony. The text and the caption for Fig. 1 give a detailed explanation.

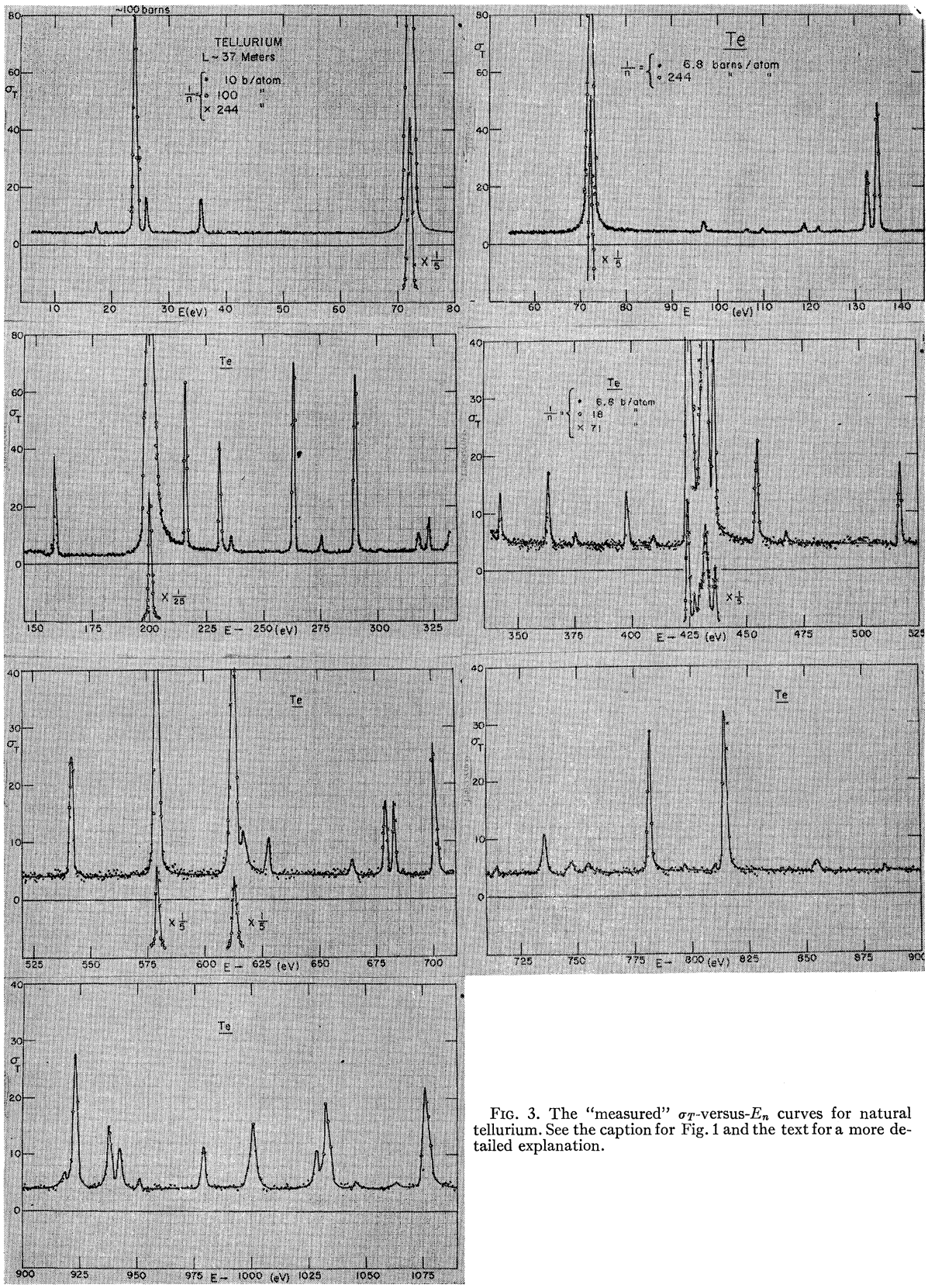

FIG. 3. The "measured" σ_T-versus-E_n curves for natural tellurium. See the caption for Fig. 1 and the text for a more detailed explanation.

TABLE II. The energies E_0 and $ag\Gamma_n^0$ values obtained for resonances in natural Sb. The letters A and B identify levels due to Sb^{121} and Sb^{123}, respectively, by other groups (see text). Levels denoted by asterisks have Γ and Γ_γ assignments established as listed in Table III.

	E_0 (eV)	ΔE_0 (eV)	$ag\Gamma_n^0$ (meV)	$\Delta ag\Gamma_n^0$ (meV)
*A	15.41	0.06	0.50	0.05
*B	21.40	0.06	1.30	0.10
*A	29.65	0.05	0.30	0.05
B	47.10	0.10	0.003	0.001
B	50.63	0.10	0.09	0.01
A	53.55	0.12	0.08	0.01
A	64.50	0.05	0.020	0.003
*A	73.79	0.05	0.25	0.03
*B	76.72	0.05	0.13	0.02
A	89.60	0.06	0.50	0.15
A	90.25	0.07	0.20	0.10
*B	104.96	0.10	1.20	0.15
A	111.35	0.10	0.085	0.005
*A	126.80	0.10	0.82	0.04
A	131.90	0.10	0.28	0.03
*A	144.22	0.10	0.34	0.03
*A	149.85	0.12	0.68	0.03
	157.10	0.06	0.004	0.001
A	160.50	0.06	0.043	0.005
*A	167.05	0.10	0.40	0.02
	176.50	0.10	0.0055	0.001
	184.60	0.10	0.003	0.0005
	186.00	0.10	0.005	0.0005
*B	191.80	0.10	0.38	0.03
	197.70	0.10	0.006	0.0005
	213.95	0.10	0.028	0.002
	218.50	0.10	0.065	0.030
*	222.60	0.10	0.11	0.02
	225.05	0.10	0.002	0.001
	230.60	0.10	0.017	0.002
*	240.55	0.10	0.29	0.02
	245.85	0.10	0.004	0.001
	248.70	0.10	0.004	0.001
	261.60	0.12	0.003	0.001
	265.70	0.12	0.005	0.001
	270.05	0.12	0.004	0.001
	274.96	0.12	0.0045	0.001
	282.70	0.12	0.002	0.001
*	286.40	0.12	0.24	0.03
	293.70	0.12	0.003	0.001
	295.90	0.12	0.02	0.003
*	299.30	0.12	0.36	0.03
	307.10	0.15	0.006	0.002
	309.33	0.15	0.035	0.005
	317.00	0.15	0.005	0.002
	320.50	0.15	0.008	0.002
	323.65	0.15	0.40	0.10
	331.40	0.15	0.11	0.02
	338.49	0.15	0.25	0.05
	339.00	0.15	0.05	0.02
	344.00	0.15	0.005	0.001
	347.17	0.15	0.003	0.002
	351.20	0.20	0.08	0.02
	355.80	0.20	0.004	0.001
	367.11	0.20	0.005	0.001
	372.96	0.20	0.010	0.002
	392.84	0.20	1.00	0.10
	394.98	0.20	0.20	0.05
	405.72	0.25	0.018	0.002
	414.58	0.25	0.014	0.002
	421.37	0.25	0.15	0.02
	443.51	0.25	0.60	0.15
	447.62	0.25	0.48	0.08
	450.23	0.25	0.60	0.10
	453.80	0.30	2.00	0.30
	470.10	0.30	0.30	0.05
	481.58	0.30	0.18	0.04
	496.98	0.30	0.08	0.02
	500.00	0.30	0.004	0.001
	507.14	0.30	0.003	0.001
	520.00	0.35	0.007	0.002
	533.10	0.35	0.07	0.02
	535.13	0.35	0.12	0.03
	543.20	0.35	1.50	0.20
	558.93	0.35	0.30	0.05
	563.45	0.35	0.013	0.002
	571.06	0.40	0.50	0.10
	577.05	0.40	0.006	0.002
	580.00	0.40	0.004	0.001
	587.00	0.40	0.008	0.002
	592.50	0.40	0.005	0.002
	599.00	0.40	0.14	0.02
	605.60	0.45	0.95	0.15
	613.45	0.45	0.14	0.03
	627.60	0.45	0.26	0.03
	630.83	0.45	0.33	0.03
	644.00	0.45	0.002	0.001
	651.80	0.50	0.002	0.001
	659.10	0.50	0.25	0.10
	661.17	0.50	0.35	0.10
	665.50	0.50	0.004	0.001
	671.05	0.50	0.42	0.06
	675.80	0.50	0.17	0.03
	691.48	0.50	0.03	0.005
	697.00	0.50	0.005	0.001
	705.00	0.55	0.003	0.001
	710.50	0.55	0.21	0.05
	715.2	0.55	0.015	0.005
	718.6	0.55	0.50	0.06
	727.8	0.55	0.005	0.002
	735.3	0.55	0.10	0.02
	747.4	0.55	1.80	0.25
	754.5	0.60	0.0025	0.0005
	762.6	0.60	0.005	0.001
	772.3	0.60	1.00	0.20
	774.8	0.60	0.10	0.05
	789.7	0.60	0.25	0.05
	795.20	0.60	0.57	0.10
	800.20	0.65	0.90	0.20
	803.50	0.65	0.67	0.20
	815.50	0.65	0.37	0.05
	839.20	0.65	1.20	0.20
	859.20	0.65	0.12	0.04
	865.20	0.70	0.005	0.003
	872.00	0.70	1.80	0.30
	885.20	0.70	0.60	0.14
	889.60	0.70	0.065	0.01
	893.50	0.70	0.006	0.002
	910.80	0.70	0.25	0.10
	911.50	0.70	0.30	0.10
	917.00	0.80	1.00	0.20
	929.50	0.8	0.10	0.02
	936.2	0.8	0.025	0.005
	947.5	0.8	0.52	0.08
	952.0	0.8	0.005	0.002
	962.4	0.8	0.42	0.06
	968.7	0.8	0.20	0.04
	977.5	0.8	0.035	0.005
	983.5	0.8	0.002	0.001
	988.3	0.8	0.66	0.15
	993.5	0.8	1.00	0.20
	1012.7	0.9	0.20	0.04
	1026.3	0.9	0.09	0.02
	1032.7	0.9	0.003	0.001
	1036.4	0.9	0.06	0.02
	1048.4	0.9	0.46	0.15
	1058.0	0.9	0.003	0.002
	1072.5	0.9	0.008	0.004
	1084.5	1.0	0.44	0.10
	1110.9	1.0	1.25	0.20
	1117.5	1.0	0.25	0.06
	1123.5	1.0	0.03	0.01
	1128.2	1.0	0.01	0.005
	1145.0	1.1	0.09	0.02
	1165.0	1.1	0.58	0.06
	1180.5	1.1	0.80	0.30

TABLE II (*continued*)

E_0 (eV)	ΔE_0 (eV)	$ag\Gamma_n^0$ (meV)	$\Delta ag\Gamma_n^0$ (meV)	E_0 (eV)	ΔE_0 (eV)	$ag\Gamma_n^0$ (meV)	$\Delta ag\Gamma_n^0$ (meV)
1183.7	1.1	0.80	0.30	2024	1.4	0.04	0.02
1201.7	1.2	0.40	0.10	2035	1.4	0.42	0.10
1213.0	1.2	0.02	0.01	2045	1.4	0.01	0.01
1220.0	1.2	0.20	0.05	2053	1.4	0.05	0.02
1233.0	1.2	0.02	0.01	2085	1.4	0.22	0.05
1250.0	1.2	1.00	0.2	2107	1.5	0.60	0.10
1260.5	1.2	0.08	0.02	2115	1.5	0.28	0.05
1265.0	1.3	0.01	0.01	2148	1.5	1.00	0.20
1273.2	1.3	0.35	0.05	2153	1.5	0.60	0.20
1307.5	1.3	1.35	0.30	2172	1.5	0.40	0.10
1329.2	1.3	0.28	0.03	2190	1.5	0.04	0.02
1334.3	1.3	0.03	0.01	2196	1.5	0.03	0.02
1347.2	1.3	0.18	0.05	2204	1.5	0.15	0.05
1353.9	1.4	0.02	0.005	2222	1.5	0.30	0.10
1364.9	0.7	0.90	0.05	2237	1.5	0.85	0.20
1385.5	0.7	0.13	0.05	2250	1.5	0.01	0.01
1397.9	0.7	0.025	0.005	2255	1.5	0.35	0.05
1415.2	0.7	0.050	0.010	2268	1.5	0.22	0.04
1421.1	0.7	0.06	0.01	2274	1.5	0.03	0.02
1436.6	0.8	0.35	0.20	2280	1.5	0.03	0.02
1438.1	0.8	0.25	0.10	2305	1.6	0.55	0.10
1451.6	0.8	0.09	0.02	2315	1.6	0.10	0.02
1458.4	0.8	0.02	0.01	2325	1.6	0.02	0.01
1467.2	0.8	0.01	0.01	2335	1.6	0.01	0.01
1483.5	0.8	1.70	0.30	2346	1.6	0.02	0.01
1491.0	0.8	0.35	0.10	2357	1.6	0.30	0.05
1494.2	0.8	0.25	0.10	2366	1.6	0.50	0.10
1521.4	0.9	0.06	0.02	2375	1.6	0.04	0.02
1529.6	0.9	0.05	0.02	2384	1.6	0.03	0.02
1533.7	0.9	0.01	0.01	2394	1.6	0.40	0.08
1541.1	0.9	0.01	0.01	2411	1.7	0.03	0.02
1550.2	0.9	0.01	0.01	2419	1.7	0.01	0.01
1555.0	0.9	0.11	0.02	2431	1.7	0.01	0.01
1574.8	0.9	0.06	0.02	2436	1.7	0.35	0.05
1581.6	0.9	0.01	0.01	2444	1.7	0.05	0.02
1595.0	0.9	0.60	0.10	2462	1.7	0.20	0.04
1599.8	0.9	0.10	0.02	2473	1.7	0.03	0.01
1601.5	1.0	0.02	0.01	2479	1.7	0.25	0.05
1619.5	1.0	0.60	0.10	2500	1.8	0.04	0.02
1640.0	1.0	0.20	0.04	2509	1.8	0.03	0.02
1648.2	1.0	0.20	0.05	2526	1.8	1.50	0.50
1653.8	1.0	0.02	0.01	2533	1.8	0.17	0.03
1662.9	1.0	0.02	0.01	2538	1.8	0.03	0.02
1671.5	1.0	0.05	0.01	2552	1.8	0.04	0.02
1681.7	1.0	0.02	0.01	2560	1.8	0.18	0.03
1687.3	1.0	0.02	0.01	2570	1.8	0.03	0.02
1698.8	1.0	1.50	0.20	2572	1.8	0.03	0.02
1708.0	1.0	0.02	0.01	2586	1.8	0.05	0.02
1723.8	1.0	0.20	0.04	2604	1.9	0.15	0.03
1733.8	1.0	0.20	0.02	2615	1.9	0.06	0.02
1741.0	1.0	0.05	0.02	2627	1.9	0.12	0.05
1752.0	1.1	0.01	0.01	2641	1.9	0.05	0.02
1766.0	1.1	0.01	0.01	2652	1.9	0.04	0.02
1776.0	1.1	0.65	0.10	2658	1.9	0.05	0.03
1783.0	1.1	0.55	0.10	2666	1.9	0.03	0.03
1790.5	1.1	0.10	0.05	2686	1.9	0.40	0.15
1796.7	1.1	2.0	0.30	2705	2.0	0.50	0.15
1808.2	1.2	0.02	0.01	2716	2.0	0.17	0.06
1811.4	1.2	0.02	0.02	2755	2.0	0.02	0.02
1821.0	1.2	0.10	0.05	2767	2.0	0.27	0.05
1824.0	1.2	0.20	0.05	2777	2.0	0.05	0.03
1829.5	1.2	0.02	0.01	2802	2.1	0.03	0.03
1836.0	1.2	0.02	0.01	2810	2.1	0.04	0.02
1844.0	1.2	0.03	0.01	2825	2.1	0.25	0.05
1860.0	1.2	0.56	0.10	2834	2.1	0.10	0.05
1871.0	1.2	0.70	0.10	2850	2.1	0.37	0.10
1893.0	1.2	0.25	0.05	2874	2.1	0.14	0.05
1903.0	1.3	1.00	0.20	2885	2.1	0.05	0.03
1917.0	1.3	0.35	0.10	2895	2.1	0.13	0.05
1932.0	1.3	0.23	0.05	2915	2.2	0.80	0.15
1938.0	1.3	0.02	0.02	2942	2.2	0.05	0.03
1965	1.3	0.02	0.02	2962	2.2	0.03	0.02
1978	1.3	0.85	0.10	2974	2.2	0.20	0.05
2000	1.4	2.20	0.30	2996	2.2	1.25	0.20
2010	1.4	0.01	0.01				

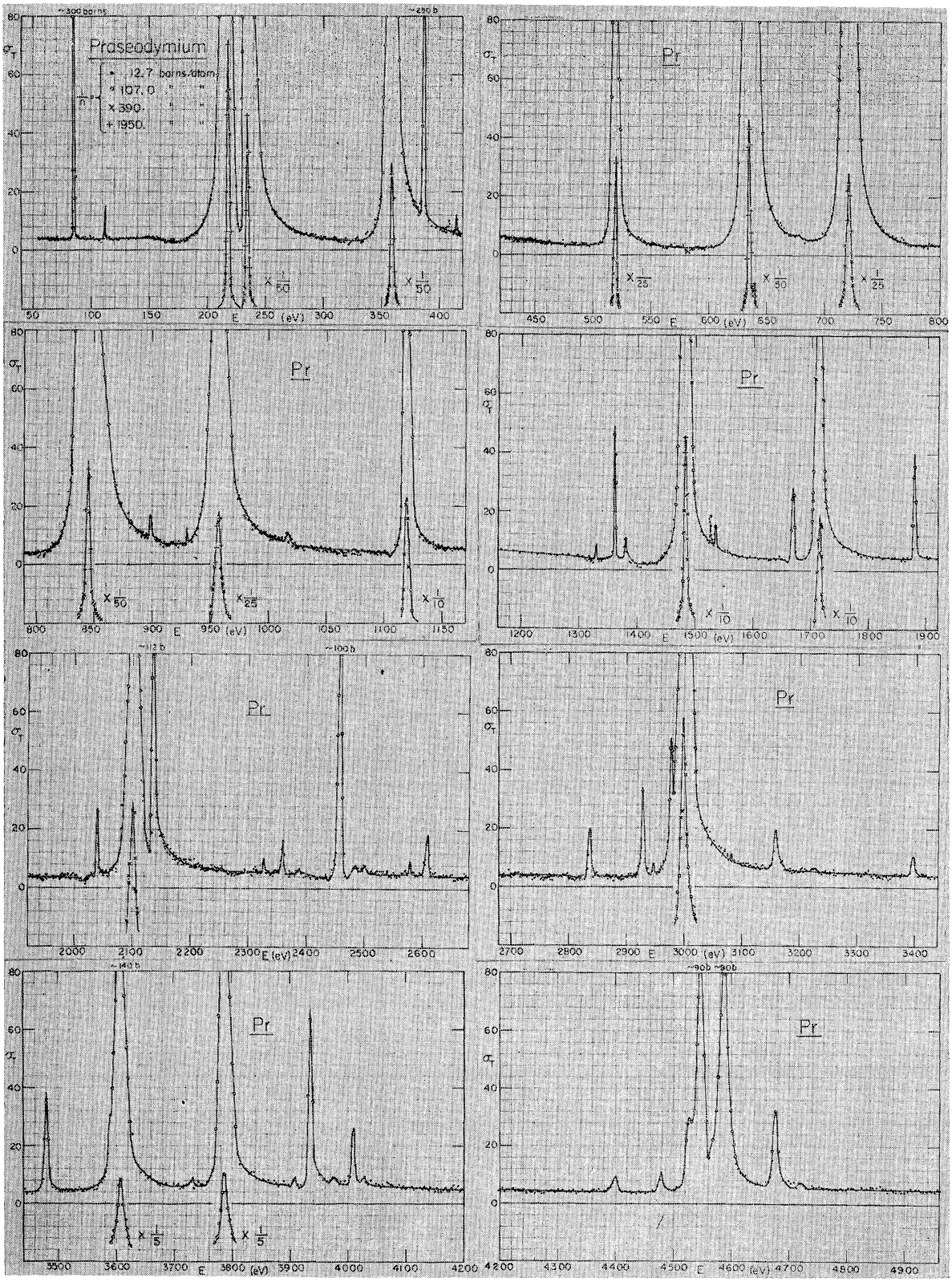

FIG. 4. The "measured" σ_T-versus-E_n curves for praseodymium. See the text and the caption for Fig. 1 for a detailed explanation.

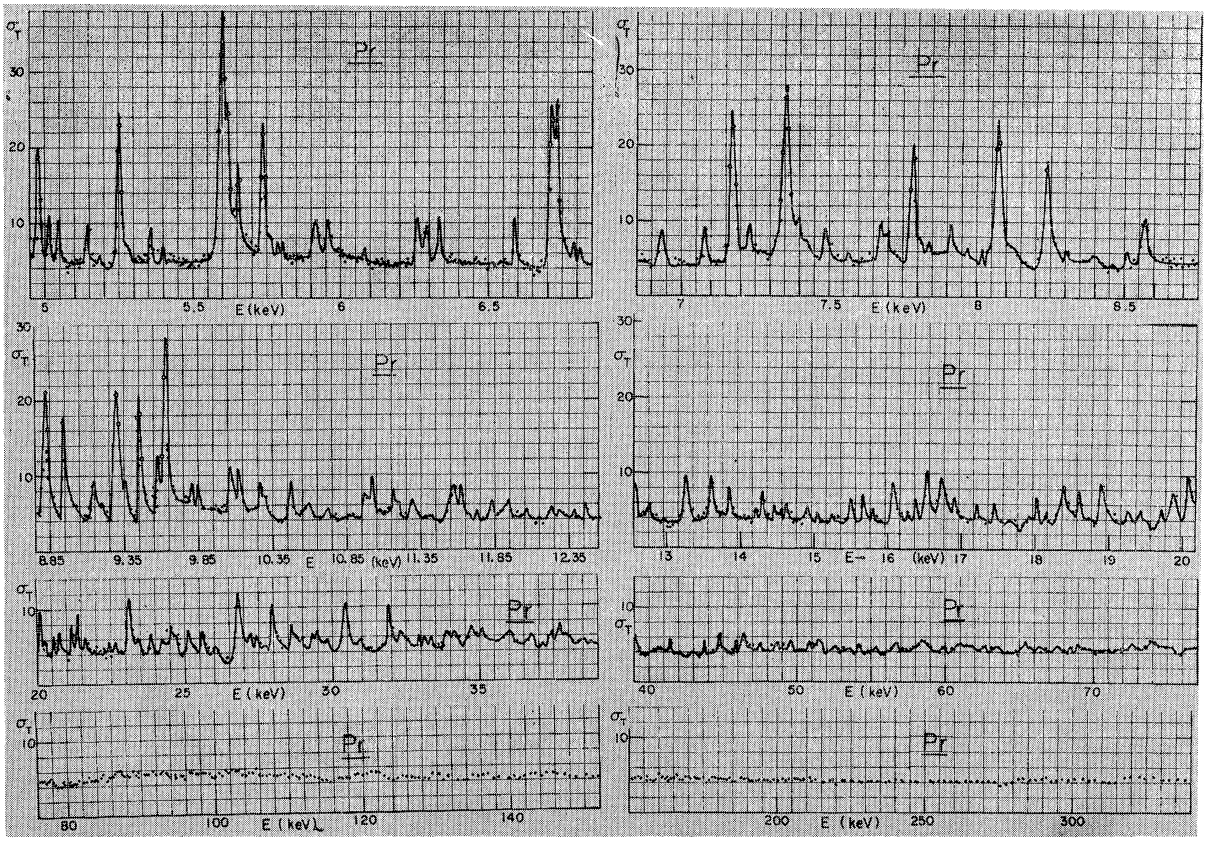

FIG. 4 (*continued*)

b/atom for regions (2) and (3); and $1/n=5.5$, 31.1, and 112 b/atom for regions (4) and (5). The measured values of the total cross section as a function of neutron energy are shown in Fig. 2 and the resonance parameters are listed in Tables II and III.

C. Tellurium

The transmission measurements for natural tellurium have been made in the same energy intervals as those for antimony under similar experimental conditions. The samples used had thicknesses corresponding to $1/n=10$, 100, and 244 b/atom for energy region (1); $1/n=6.8$ and 244 b/atom for regions (2) and (3); and $1/n=6.8$, 18, and 71 b/atom, for energy regions (4) and (5). The thick samples were of natural metal and the thinner samples were of TeO_2 mixed with sulphur as a binder. The observed transmission values were corrected for the presence of oxygen and sulphur.

The measured σ_T-versus-neutron-energy curves are shown in Fig. 3 and the resonance parameters are listed in Table IV.

D. Praseodymium

The total-neutron-cross-section measurements on praseodymium have been made over the energy interval from 50 eV to 250 keV. These measurements have been performed in three consecutive years with different conditions and the results presented here are the averages of these measurements. A flight path of 200 m with 0.1-μsec channel width was used for the highest-energy interval. Sample thicknesses having $1/n=12.7$, 25, 107, 390, and 1950 b/atom were used. The thick

TABLE III. The values of Γ and Γ_γ for those levels of natural Sb indicated by asterisks in Table II. The letters A and B have the same meaning as in Table II.

E_0 (eV)	$\Gamma\pm\Delta\Gamma$ (meV)	$\Gamma_\gamma\pm\Delta\Gamma_\gamma$ (meV)
A 15.41	100±10	92±10
B 21.40	125±10	100±10
A 29.65	80±20	74±20
A 73.79	115±15	106±15
B 76.72	120±15	115±15
B 104.96	120±15	71±15
A 126.80	115±20	78±20
A 144.22	110±15	94±15
A 149.85	150±25	117±25
A 167.05	120±30	99±30
B 191.80	130±20	109±20
222.60	150±20	143±20
240.55	140±20	122±20
286.40	135±25	119±25
299.30	145±20	120±20

TABLE IV. The energies E_0 and $ag\Gamma_n^0$ values for levels in natural Te. The letters A, B, C, D refer to isotope assignments made by others (see text) for $A=122$, 123, 124, 125, respectively.

	E_0 (eV)	ΔE_0 (eV)	$ag\Gamma_n^0$ (meV)	$\Delta ag\Gamma_n^0$ (meV)
	17.26	0.03		
B	24.19	0.04	0.11	0.02
D	26.34	0.04	0.008	0.001
B	35.93	0.07	0.01	0.002
A	72.79	0.03	1.0	0.2
B	96.92	0.05	0.006	0.001
	106.10	0.06	0.002	0.001
B	109.83	0.06	0.0027	0.001
B	119.00	0.07	0.0047	0.001
	121.97	0.07	0.002	0.001
B	132.90	0.08	0.06	0.01
D	135.02	0.09	0.08	0.02
B	158.75	0.05	0.05	0.01
C	200.57	0.07	3.9	0.4
D	216.02	0.09	0.17	0.01
A,D	230.91	0.10	0.14	0.05
B	235.30	0.10	0.015	0.004
D	263.10	0.11	0.16	0.05
B	275.09	0.12	0.019	0.005
D	289.89	0.13	0.18	0.05
	301.01	0.14	0.004	0.001
	317.84	0.15	0.02	0.01
D	322.22	0.16	0.046	0.016
A	333.43	0.17	0.13	0.03
B	342.09	0.17	0.038	0.010
B	363.48	0.19	0.083	0.017
	374.74	0.20	0.013	0.003
D	398.00	0.22	0.05	0.016
	409.32	0.23	0.01	0.005
D	424.46	0.24	0.39	0.16
	427.59	0.24	0.059	0.009
	430.02	0.24	0.015	0.01
	432.47	0.25	0.38	0.20
	436.43	0.25	0.16	0.05
A	455.24	0.26	0.15	0.05
	467.44	0.28	0.013	0.003
D	517.29	0.30	0.095	0.005
C	541.97	0.35	0.17	0.02
	579.75	0.40	1.10	0.15
	613.23	0.42	1.15	0.20
	617.40	0.42	0.03	0.01
	628.47	0.43	0.085	0.035
	664.90	0.47	0.035	0.005
	679.69	0.49	0.09	0.02
	683.10	0.50	0.065	0.010
	700.50	0.50	0.22	0.02
	714.43	0.50	0.008	0.004
	735.26	0.55	0.105	0.005
	747.41	0.55	0.023	0.005
	754.70	0.55	0.033	0.007
	782.13	0.60	0.38	0.05
	796.70	0.60	0.013	0.005
	811.05	0.65	0.006	0.006
	815.49	0.65	0.34	0.05
	855.12	0.70	0.04	0.01
	885.32	0.75	0.01	0.01
	918.68	0.75	0.01	0.01
	923.37	0.75	0.39	0.05
	938.03	0.80	0.13	0.02
	942.77	0.80	0.055	0.015
	951.54	0.80	0.03	0.01
	979.46	0.85	0.12	0.02
	1000.77	0.85	0.26	0.04
	1029.09	0.90	0.05	0.01
	1032.71	0.90	0.65	0.15
	1045.54	0.95	0.013	0.005
	1063.35	0.95	0.06	0.02
	1076.76	0.95	0.64	0.04
	1099.30	1.00	0.12	0.02
	1128.86	1.05	0.41	0.05
	1141.42	1.05	0.11	0.02
	1189.32	1.15	0.083	0.016
	1249.91	1.20	0.13	0.05
	1310.05	1.30	0.020	0.005
	1316.56	1.30	0.15	0.03
	1321.15	1.30	0.03	0.01
	1330.39	0.65	0.01	0.005
	1360.10	0.70	0.17	0.04
	1363.54	0.70	0.05	0.01
	1439.60	0.75	0.017	0.01
	1450.89	0.75	0.068	0.023
	1461.54	0.75	0.9	0.3
	1522.24	0.80	0.15	0.02
	1534.51	0.80	0.03	0.02
	1540.28	0.85	0.078	0.006
	1549.09	0.85	0.03	0.01
	1556.96	0.85	2.85	0.30
	1574.76	0.85	0.03	0.01
	1585.08	0.85	0.08	0.02
	1596.40	0.90	0.03	0.01
	1629.15	0.90	0.063	0.015
	1650.00	0.90	0.05	0.03
	1684.52	0.95	0.06	0.01
	1692.11	0.95	0.19	0.02
	1698.80	0.95	0.045	0.010
	1714.23	0.95	0.35	0.10
	1728.89	1.00	0.10	0.05
	1749.74	1.00	0.55	0.20
	1755.76	1.00	0.065	0.025
	1776.07	1.05	0.023	0.005
	1785.33	1.05	0.21	0.04
	1806.15	1.05	0.21	0.06
	1813.53	1.05	0.02	0.02
	1839.16	1.10	3.9	0.4
	1904.53	1.15	0.09	0.02
	1914.81	1.15	0.03	0.01
	1934.45	1.15	0.18	0.03
	1992.79	1.20	4.00	0.5
	2027.32	1.25	0.26	0.09
	2056.36	1.25	0.15	0.05
	2093.87	1.30	0.05	0.01
	2150.04	1.35	0.16	0.03
	2207.08	1.40	0.05	0.02
	2215.62	1.45	0.03	0.02
	2275.31	1.50	0.8	0.2
	2314.43	1.50	0.11	0.04
	2328.20	1.55	0.21	0.05
	2375.01	1.60	0.60	0.12
	2382.95	1.60	1.1	0.2
	2495.00	1.70	0.10	0.03
	2524.25	1.75	15.5	2.5
	2598.74	1.80	0.30	0 10
	2606.01	1.80	1.2	0.15
	2631.69	1.85	0.80	0.1
	2640.95	1.85	0.2	0.2
	2742.20	1.95	0.55	0.18
	2789.98	2.0	0.2	0.04
	2832.81	2.1	0.72	0.1
	2849.4	2.1	0.4	0.05
	2870.3	2.1	0.33	0.08
	2923.7	2.2	0.15	0.10
	2941.0	2.2	2.4	0.8
	2974.1	2.2	4.6	1.5
	3123.8	2.3	0.25	0.05
	3191.7	2.5	0.5	0.2
	3201.6	2.5	0.29	0.01
	3269.6	2.5	0.45	0.15
	3303.1	2.6	0.35	0.05
	3337.2	2.6	0.22	0.03
	3393.3	2.7	0.75	0.10
	3442.5	2.7	0.55	0.10
	3490.0	2.8	0.29	0.16
	3544.2	2.9	0.12	0.04
	3552.9	2.9	0.16	0.04

TABLE IV (*continued*)

E_0 (eV)	ΔE_0 (eV)	$ag\Gamma_n^0$ (meV)	$\Delta ag\Gamma_n^0$ (meV)	E_0 (eV)	ΔE_0 (eV)	$ag\Gamma_n^0$ (meV)	$\Delta ag\Gamma_n^0$ (meV)
3587.9	3.0	0.50	0.10	4234.5	3.8	0.35	0.10
3650.5	3.0	0.07	0.02	4253.4	3.8	0.12	0.02
3683.9	3.1	0.08	0.02	4283.9	3.8	0.20	0.05
3711.6	3.1	0.28	0.10	4401.4	4.0	0.30	0.15
3787.0	3.1	0.076	0.015	4449.7	4.1	0.70	0.15
3825.5	3.2	0.30	0.05	4482.4	4.1	0.12	0.08
3854.8	3.3	1.40	0.40	4515.4	4.2	0.10	0.05
3992.7	3.5	0.19	0.05	4569.9	4.2	0.80	0.20
4010.0	3.5	0.37	0.05	4602.0	4.2	0.05	0.05
4062.7	3.5	0.14	0.05	4638.3	4.3	0.20	0.10
4087.6	3.6	0.25	0.10	4677.5	4.4	0.10	0.05
4193.3	3.7	0.06	0.06	4770.8	4.5	0.25	0.05
4219.4	3.8	0.16	0.05	4862.2	4.6	0.5	0.2

sample was natural metal, and thinner samples were of PrO_2 mixed with sulphur as a binder. The correction in the transmission due to the presence of oxygen and sulphur has been made. A plot of the observed σ_T versus E_n is shown in Fig. 4, and the resonance parameters are given in Table V.

E. Level Parameter Analysis

Figures 5(a) and 5(b) show examples of the area analysis for the levels in Sb at 144.22 and 240.55 eV. The measured transmission dip for each sample $(1/n)$ value implies the indicated functional dependence of $ag\Gamma_n^0$ on an assumed Γ. For the "thin" samples [large $(1/n)$ for a strong level], the implied $ag\Gamma_n^0$ value is relatively independent of the choice of Γ. For a thicker sample where the effect of the interference between potential and resonance scattering is not excessive, the quantity $ag\Gamma_n^0\Gamma^s(0<s<1)$ tends to be established. As the sample thickness increases, the curves have an increasingly rapid decrease of implied $ag\Gamma_n^0$ with increasing assumed Γ. The "thin" samples tend to have

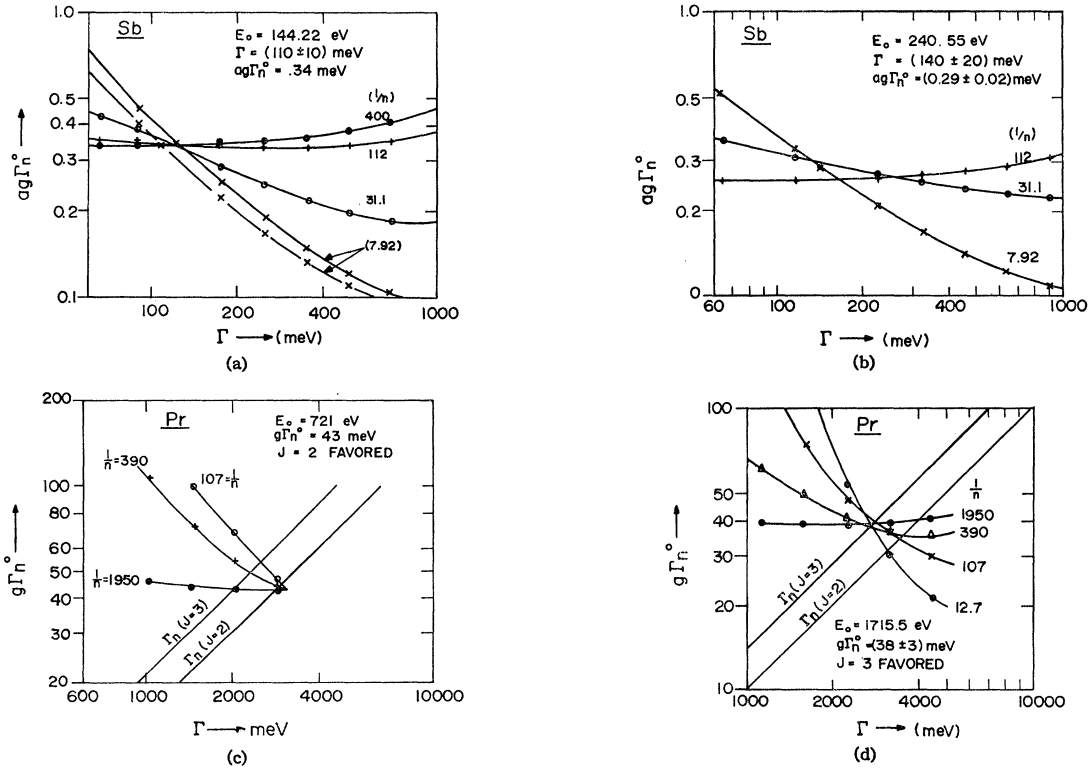

FIG. 5. Examples of the determination of the resonance parameters for two favorable resonances each in natural Sb and Pr. The measured "area" of the transmission dip for each sample $(1/n)$ value implies a particular functional relationship between $ag\Gamma_n^0$ and (assumed) Γ. If the curves have a well-defined common point of intersection, that is the favored $(ag\Gamma_n^0,\Gamma)$ solution. For (c) and (d) the $J=2$ and $J=3$ lines give the contribution of Γ_n to Γ for the two possible J choices. The solution point must be a distance $\Gamma_\gamma \approx 100$ meV to the right of the curve for the proper J value.

TABLE V. The observed level parameters for natural Pr. Labels A and B denote assignment to favored spin states $J=2$ and $J=3$, respectively. Levels marked with an asterisk are uncertain and could be due to spurious statistical data fluctuations. Note: Our observed levels at energies above 10 keV are listed elsewhere,[a] but all these quoted resonance energies (E_0) should be lowered by the stated value of the energy uncertainty.

	E_0 (eV)	ΔE_0 (eV)	$ag\Gamma_n^0$ (meV)	$\Delta ag\Gamma_n^0$ (meV)
	85.24	0.10	0.72	0.05
	112.33	0.10	0.031	0.005
B	218.65	0.15	90	10
A	235.20	0.15	66	8
B	359.70	0.20	74	6
	387.90	0.20	3	1
	415.10	0.20	0.05	0.02
A	519.6	0.50	38	4
B	635.4	0.50	120	20
*	639.0	0.80		
A	721.0	1	88	10
B	845.2	1	200	32
	899	1	0.26	0.03
	931.5	1	0.10	0.03
A	957.2	1	110	10
	1017.0	1	0.14	0.04
	1120.0	1	36	6
*	1285.0	1	0.1	0.1
	1331.0	1	0.15	0.05
	1364	1	2.8	0.4
	1384	1.5	0.3	0.1
A	1484	1.5	114	20
*	1529	1.5	0.1	0.1
	1537	1.5	0.4	0.2
	1672	1.5	1.4	0.2
B	1715.5	1.5	76	6
(A)	1880	2	3.3	0.4
	2036	2	3.5	0.5
B	2096	2	160	16
	2132	2	23	4
	2324	2	0.3	0.1
	2356	2	2	0.2
B	2452	2.5	34	4
*	2498	2.5	0.2	0.1
	2576	2.5	0.5	0.1
	2605	2.5	5.0	1.0
*	2706	2.5	0.1	0.1
*	2789	3.0	0.2	0.1
	2835	3.0	2.7	0.4
B	2926	3.0	9.4	1.0
	2944	3.0	0.4	0.2
	2977	3.0	5.0	2.0
B	2998	3.0	240	40
	3079	3.0	0.3	0.2
A	3156	3.0	10.4	2.0
*	3182	3.0	0.1	0.1
	3223	3.0	0.2	0.2
	3396	3.0	2.2	0.4
(B)	3474	3.0	16	2
	3582	3.5	8	4
(B)	3603	3.5	130	20
*	3643	3.5	0.2	0.2
	3726	3.5	0.8	0.4
(B)	3780	3.5	148.0	20
	3902	3.5	0.6	0.2
(A)	3928	3.5	27	5
	3970	4	0.7	0.2
(A)	4002	4	9.0	2
	4397	4	4	1
	4476	4	4	1
	4522	4	10	5
	4544	4	80	20
	4587	4	80	16
	4598	4	0.1	0.1
	4673	4	12	4
	4699	4	0.64	0.2
	4744	4	0.1	0.1
	4766	4	0.1	0.1
	4977	5	10.0	1.0
	5011	5	4.0	1.0
	5043	5	2.2	0.4
	5143	5	3.6	0.4
	5178	5	0.6	0.3
	5250	5	40	8
	5356	5	2.5	0.4
	5395	5	0.2	0.2
	5510	5	0.45	0.1
	5600	6	150	30
	5612	6		
	5646	6	20	10
	5734	6	40	8
	5784	6	0.3	0.1
	5802	6	0.3	0.1
	5914	6	6.0	1
	5954	6	5.0	0.5
	5998	7	0.3	0.1
	6073	7	0.4	0.1
	6255	7	5	1
	6286	7	4	1
	6329	7	5	1
	6456	7	0.6	0.3
	6582	8	6	1
	6711	8	60	15
	6726	8	40	12
	6779	8	0.8	0.4
	6927	8	5	1
	7076	9	4.0	1.0
	7169	9	50	10
	7221	9	3.0	0.5
	7347	9	100	25
	7391	9	0.4	0.2
	7483	9	4.0	1.0
	7558	10	0.5	0.2
	7667	10	6	2
	7693	10	4	2
	7779	10	44	10
	7830	10	1.0	0.2
	7903	10	5.0	1
	7960	10	0.4	0.2
	8010	10	0.8	0.3
	8062	11	60	15
	8119	11	1.0	0.5
	8229	11	36	8
	8291	11	0.5	0.2
	8333	11	2	1
	8387	11	2	1
	8502	11	3	1
	8555	12	14	2
	8804	12	90	16
	8925	12	56	20
	9113	12	36	8
	9258	12	100	25
	9338	12		
	9443	13	112	30
	9544	13		
	9557	13	60	15
	9621	13	160	40
	9792	13		
	9822	13	10	2
	9899	13		
	10049	13	50	10

[a] Reference 3.

smaller and narrower dips and their areas may have large statistical uncertainty. (For weak levels even the thickest sample will be "thin" and may be the only one to show the level.)

The evaluation[1] of the "area" of the transmission dip requires a knowledge of the transmission in the neighborhood of a resonance due to all contributions to the cross section *except* that due to a resonance under investigation. There is some uncertainty in establishing this transmission value for the thick samples, particularly if there is a large energy-dependent contribution from one or more neighboring levels. In Fig. 5(a) the two curves for the thickest sample represent extreme limits and the over-all evaluation gives $\Gamma=110\pm10$ meV, $ag\Gamma_n^0=0.34$ meV. Subtracting $4ag\Gamma_n$ from Γ gives $\Gamma_\gamma=94\pm15$ meV.

In Fig. 5(b) there is no common intersection of the curves for the three samples, but the intersection of the curve for $(1/n)=7.92$ with the other two limits the range of acceptable Γ values between 120 and 160 meV.

Figure 5(c) shows the analysis for the level in Pr at 721 eV. Since $a=1$ and $g=5/12$ or $7/12$, respectively, for $J=2$ or 3, one can construct two curves of Γ_n (abscissa) versus $g\Gamma_n^0$ (ordinate). A self-consistent choice of $g\Gamma_n^0$ and Γ must correspond to a point at a distance equal to Γ_γ to the right of the proper Γ_n line. A survey of the best determinations of Γ_γ values for the Pr levels shows that $\Gamma_\gamma\sim80$ to 100 meV is favored. In Fig. 5(c) the three sample thickness curves intersect at $g\Gamma_n^0=43$ meV, $\Gamma\approx3000$ meV. The $J=2$ line gives a good fit, but the $J=3$ line misses by about 1000 meV for Γ. The $J=2$ assignment here agrees with that reported by Julien *et al.*[3] It is evident that the determination of a favored J value is only possible if the two implied values of Γ_n lead to appreciably different values of Γ_γ. This condition only applies for strong levels.

Figure 5(d) shows the analysis for the level in Pr at 1715.5 eV. The intersection of the various curves is not at a common point. One now includes the consistency condition for $\Gamma_\gamma\sim80$ to 100 meV. The acceptable solution is a point on the plot which should be ~100 meV to the right of either the $J=3$ or $J=2$ curve. The $J=2$ curve is obviously a bad choice, but $g\Gamma_n^0=38\pm3$ meV, $\Gamma\approx2800$ meV is consistent with the data and with the $J=3$ condition. This choice of $J=3$ agrees with that of Julien *et al.*[3] for this resonance. A number of J assignments for resonances in Pr have been obtained using this procedure.

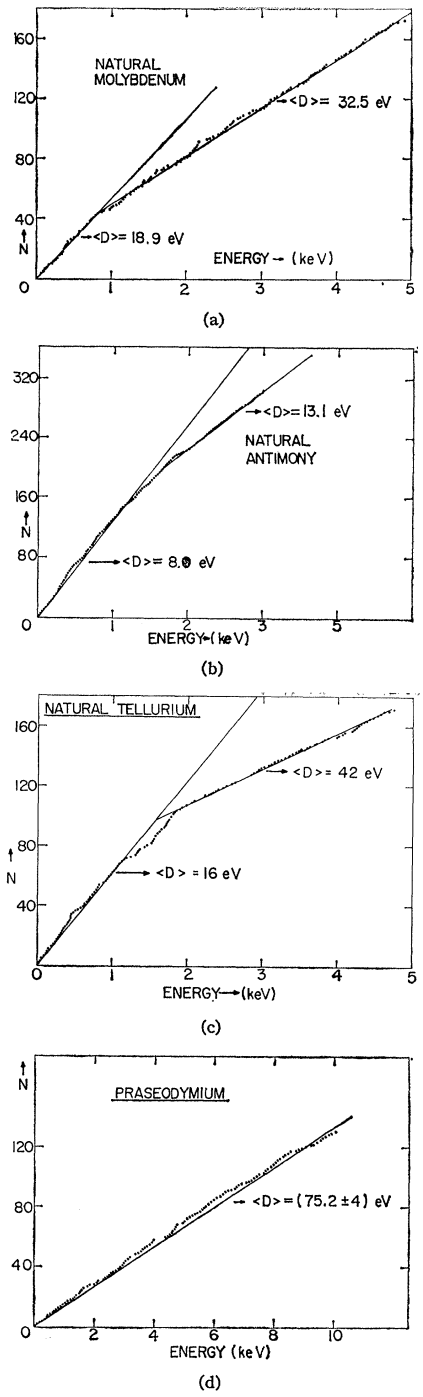

FIG. 6. A plot of the number of levels observed in (a) natural Mo, (b) natural Sb, (c) natural Te, and (d) Pr as a function of the upper energy. The slopes of the plots correspond to the observed level densities.

III. DISCUSSION OF RESULTS

A. Mean Level Spacings and the $l=0$ Strength Function

Figures 6(a)–6(d) show the number of resonances observed versus neutron energy for Mo, Sb, Te, and Pr, respectively. The slope of each curve represents the observed level density as a function of energy. At higher energies the decrease in slope represents a decreasing efficiency for detecting resonances, so such plots are helpful for establishing the energy interval over which most levels are detected for establishing "observed" mean level spacings $\bar{D}$ for the elements.

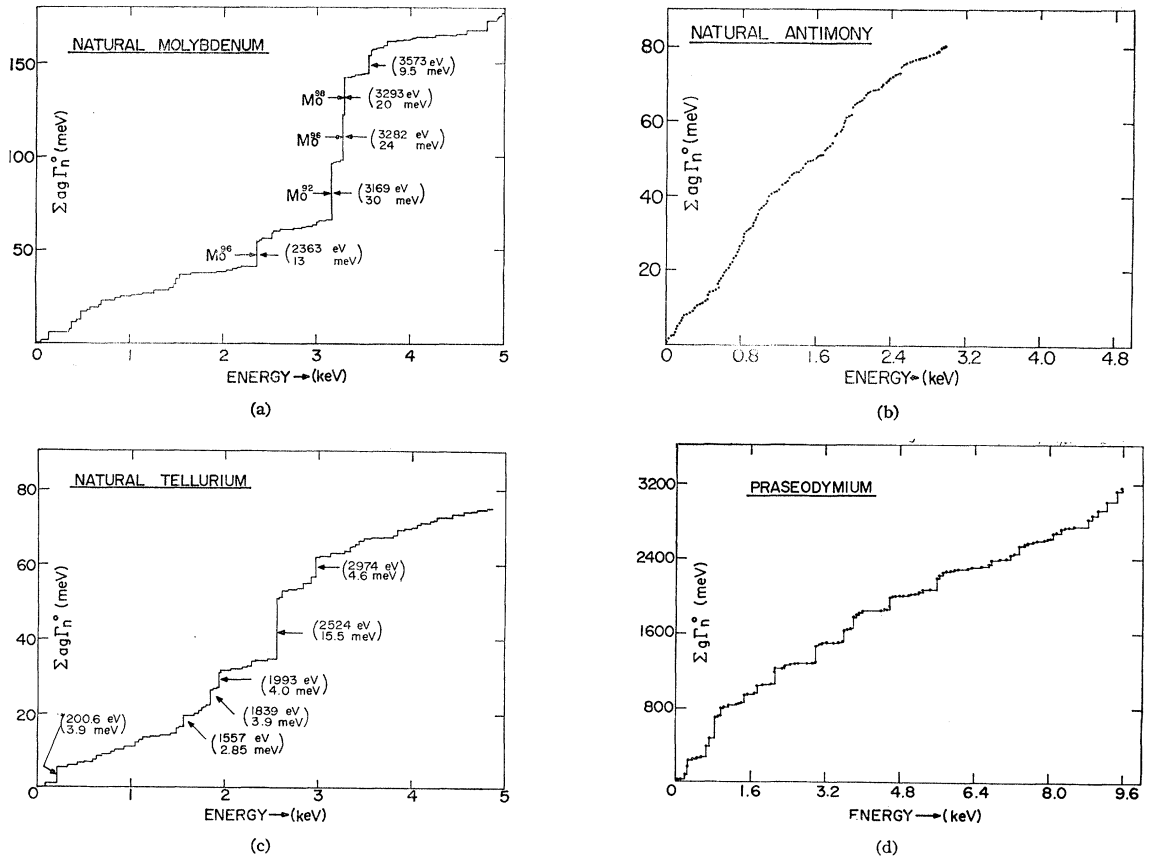

FIG. 7. Plots of $\sum ag\Gamma_n^0$ versus neutron energy for (a) natural Mo, (b) natural Sb, (c) natural Te, and (d) Pr. The slopes correspond to the strength function S_0.

Contributions from all naturally present isotopes and both $l=0$ and relatively strong $l=1$ levels are present for all possible compound-nucleus J values consistent with $l=0$ (or $l=1$) for the incoming neutrons. A few of the very weak "observed" levels are probably spurious and reflect large statistical fluctuations in the data numbers. This has been discussed in previous papers.[1]

When, as is probably true for Mo, Sb, and Te, there is a significant $l=1$ population contribution to the observed level density, this contribution will be important mainly at lower energies where weak (very small $ag\Gamma_n^0$) levels are more likely to be detected as discussed in previous papers.[1] When one inquires about the "true" level density or the mean level spacing $\langle D\rangle$ in such a situation, one must use a more detailed specification of the quantity of interest. If $\langle D\rangle$ is desired for the $l=0$ population only, then the lowest-energy region is apt to include a significant contribution from $l=1$ levels which, however, cannot (individually) be identified in terms of $l=0$ or 1. The fraction of the observed levels due to $l=1$ increases as one improves the measurement resolution and the statistical accuracy of the data, or adopts methods (such as the observation of capture γ rays) which are particularly sensitive for locating weak (capture) levels. In Figs. 6(a)–6(c) the $l=0$ population-level densities are expected to be somewhere between the values given by the slopes at the lowest and highest energies. Because of the smallness of the centrifugal-barrier penetration factor, it is unlikely that one can achieve a count of all $l=1$ levels over a significant energy region for $E\lesssim 10$ keV.

TABLE VI. S-wave strength functions for different isotopes of Mo using the isotope assignments of Pevsner *et al.*[a]

Isotope	Number of Resonances	$S_0\times10^{-4}$
Mo^{95}	12	0.38±0.15
Mo^{97}	10	0.8 ±0.4
Mo^{98}	7	0.41±0.24
Mo^{100}	6	0.21±0.12

[a] Reference 4.

In the case of Pr the $l=0$ neutrons contribute to two populations having $J=3$ and $J=2$. For Sb the two natural isotopes each have nearly 50% abundance and $I=\frac{5}{2}$ (Sb^{121}) and $\frac{7}{2}$ (Sb^{123}), so four "spin-isotope" populations are present with comparable "sample weightings." For Mo and Te, however, there are many isotopes of both odd and even A values with widely varying abundances and mean level spacings, so that it is likely that we are missing a considerable number

of levels of the less abundant isotopes. The even-A isotopes tend to have fewer, but stronger, levels which are more apt to be observed and may contribute abnormally to the measured strength function (as is discussed below). There is information as to the isotopic identification of a number of the lower-energy resonances which permits some estimate of the contribution of the different isotopes to the observed level density for the natural elements.

With the above considerations in mind we note that Figs. 6 (a)–6(d) give the following results:

$\langle D\rangle = 18.9$ eV for the 42 levels of natural Mo below 800 eV. A value $\langle D\rangle = 31.2$ eV is obtained for the relatively straight region of Fig. 6(a) for 800 eV $\leq E \leq 4700$ eV.

$\langle D\rangle = 8.0$ eV for natural Sb if the portion of Fig. 6(b) below 1200 eV is used. For the relatively straight region below 800 and 1800 eV the slope gives $\langle D\rangle = 10.6$ eV, while the relatively straight region from 1.8 to 3 keV gives $\langle D\rangle = 13.1$ eV.

$\langle D\rangle = 16$ eV for natural Te using the relatively straight portion of Fig. 6(c) below 1100 eV. However, the relatively straight region from 1.8 to 4.6 keV gives $\langle D\rangle = 42$ eV.

$\langle D\rangle = 75.2 \pm 4$ eV for Pr using the full linear region of the plot of Fig. 6(d) for E up to 10 keV. Since the full energy range gives a reasonably consistent straight-line plot, a quoted uncertainty is given in this case, using the formula $[(4-\pi)/\pi n]^{1/2}\langle D\rangle$. However, as discussed later, the fit of the $g\Gamma_n^0$ distribution to the Porter-Thomas theory is poor, with an excess of weak levels. The interpretation of the $\langle D\rangle$ value as due to an $l=0$ population only is considered in more detail in a later section.

Figures 7(a)–7(d) show plots of $\sum ag\Gamma_n^0$ versus the upper energy limit for the four elements. The curve for natural Mo is remarkable for the large discontinuities due to contributions from a few unusually strong levels. The four strongest levels are at 2363 eV ($ag\Gamma_n^0 = 13$ meV), 3169 eV ($ag\Gamma_n^0 = 30$ meV), 3282 eV ($ag\Gamma_n^0 = 24$ meV), and 3293 eV ($ag\Gamma_n^0 = 20$ meV). They have been identified as belonging to Mo^{96}, Mo^{92}, Mo^{96}, and Mo^{98}, respectively.[4] The level at 3573 eV ($ag\Gamma_n^0 = 9.5$ meV) is probably also due to an even-A isotope. These five levels, representing $\sim 3\%$ of the levels, contribute $\sim 55\%$ of $\sum ag\Gamma_n^0$ for the region to 5 keV. For a Porter-Thomas single-population Γ_n^0 distribution it should require the strongest 15% of the levels to contain 55% of the total contribution to $\sum ag\Gamma_n^0$. The three strongest levels, contributing $\sim 42\%$ of $\sum ag\Gamma_n^0$, are concentrated in a 124-eV interval. The even isotopes compose 64% of the natural Mo atoms which is close to the 55% contribution of these five levels. There will be some additional contributions to $\sum ag\Gamma_n^0$ due to the even-A isotopes, but the remaining portion is mainly due to levels of the odd-A isotopes. Thus, our particular energy-interval sample yields essentially equal isotope average S_0 values (natural element average) for the odd and even isotopes separately. To the extent that one believes that S_0 should contain no systematic odd-even isotope difference in a given A region, our resulting S_0 value should provide a good natural element average in spite of the relatively large contribution to $\Sigma ag\Gamma_n^0$ of a few even-A isotope resonances.

A value of $S_0 = (0.35 \pm 0.06) \times 10^{-4}$ is obtained for Mo. The indicated uncertainty is larger than that expected using the formula $\Delta S_0 = 1.5n^{-1/2}S_0$. Our result is much smaller than the 1966 "recommended" value $S_0 = (0.6 \pm 0.15) \times 10^{-4}$ selected by Seth[5] after reviewing the available measurements which gave values ranging from $(0.2 \pm 0.2) \times 10^{-4}$ to 0.7×10^{-4}. Our value for Mo is close to our value[1] of $(0.40 \pm 0.09) \times 10^{-4}$ for the neighboring element Nb ($Z = 41$, $A = 93$).

Since isotope identifications are given for many of the low-energy Mo resonances, it is possible to give S_0 for these cases, noting the smallness of the population sample. The results are shown in Table VI with an indication of the number of levels used in each case.

The slope in Fig. 7(b) for natural Sb decreases systematically in the upper half of the energy interval. This may partly be attributed to loss of levels at higher energies. With this consideration in mind, we choose $S_0 = (0.34 \pm 0.05) \times 10^{-4}$ for natural Sb. The energy region (0–1.0) keV gives $S_0 = 0.36 \times 10^{-4}$ while the region (0–2.5) keV gives $S_0 = 0.29 \times 10^{-4}$. Our stated uncertainty is larger than the factor $1.5n^{-1/2}S_0$. This S_0 value for Sb is nearly equal to our values for Mo and Nb.

Figure 7(c) for natural Te also shows abnormally large contributions from the few strongest levels, although in a less extreme manner than for Mo. The even-A isotopes constitute 92% of the natural Te atoms. Although Te^{123} and Te^{125} contribute strongly to the observed element-level density, the measured S_0 will be due mainly to the even isotopes. Isotope assignments for individual levels have not been made in Table III above about 600 eV, so we have made no attempt to obtain S_0 values for the individual isotopes using our data. A value $S_0 = (0.15 \pm 0.03) \times 10^{-4}$ is our best choice for the energy interval to 5 keV. The quoted uncertainty

TABLE VII. S-wave strength functions for Pr determined using different upper energy limits for the region considered.

Energy interval (keV)	Number of levels	$S_0 \times 10^{-4}$
0–2	27	2.57±0.78
0–4	57	2.32±0.46
0–5.8	81	2.01±0.36
0–8	108	1.68±0.29
0–10	125	1.72±0.25

[4] M. I. Pevsner, Yu. V. Adamchuk, L. S. Danelyan, B. V. Efimov, S. S. Moskalev, and G. V. Muradyan, Zh. Eksperim. i Teor. Fiz. 44, 1187 (1963) [English transl.: Soviet Phys—JETP, 17, 803 (1963)].

[5] K. K. Seth, Nucl. Data, A2, 299 (1966).

TABLE VIII. Comparison of the results for some resonances in Sb with those of other experimenters as indicated.

E_0 (eV)	A	$2g\Gamma_n^0$ (meV)	Γ_γ (meV)	Reference
15.41		1.73±0.17	92±10	this paper
	121	1.9		7
		1.53±0.15	109±20	9
		1.73±0.10	88±10	10
21.40		6.1 ±0.5	100±10	this paper
	123	5.2		7
		5.4 ±0.6	86±20	9
		7.6 ±0.4	58±10	10
29.65		1.04±0.17	74±20	this paper
	121	1.2		7
		0.90±0.09	123±40	9
		0.83±0.06	89±10	10
50.63		0.42±0.04		this paper
	123	0.7		7
53.55		0.28±0.03		this paper
	121	0.4		7
64.50		0.07±0.01		this paper
	121	0.12		7
73.79		0.87±0.10	106±15	this paper
	121	1.0		7
76.72		0.61±0.08	115±15	this paper
	123	1.8		7
89.6 and 90.25	121	2.4 ±0.09		this paper
		3.3		7

is based on statistical uncertainties due to the sample size and mixed population character. This value contrasts with the much larger "recommended value" $S_0=(0.5\pm0.2)\times10^{-4}$ for natural Te chosen by Seth.[5] $S_0\sim0.10\times10^{-4}$ is obtained using the energy interval to 1400 eV before the following series of stronger levels is reached. A value of $S_0=0.32\times10^{-4}$ results using the energy region from 1.5 to 3.0 keV which contains the greatest average slope.

Figure 7(d) for Pr shows an interesting "staircase" structure with a distinctly reduced slope in the upper half of the energy interval (5–10 keV). The value obtained for S_0 will thus decrease with the size of the interval chosen. We conclude that this effect is probably real. Values of S_0 for different choices of the upper limit for the energy interval are shown in Table VII. A choice of an energy interval 5–10 keV would give $S_0\sim1.2\times10^{-4}$.

Neutron total-cross-section measurements for Pr have previously been made by several investigators. The most recent of these are the unpublished results of Julien *et al.* which are, however, included in the latest revision[3] of BNL-325. Their measurements were made at about the same time as ours and with comparable energy resolution. Our general agreement for the energies and $g\Gamma_n^0$ values for the levels to ~6 keV is excellent and reassuring. For the energy interval 0–5.8 keV they obtain $S_0=(2.1\pm0.4)\times10^{-4}$ which compares with our value of $S_0=(2.01\pm0.36)\times10^{-4}$ for the same interval. Our result for 0–10 keV is $S_0=(1.72\pm0.25)\times10^{-4}$.

B. Comparison with Other Measurements

A general compilation of all results by different investigators is contained in Ref. 3. Some of the main features are summarized below.

The identification of the isotopes responsible for many of the lower-energy resonances of the Mo isotopes was made by Pevsner *et al.*[4] in 1963. They used an electron linac pulsed neutron source at $\gtrsim$6-nsec/m resolution for transmission (total-cross-section) measurements on separated isotope samples and natural Mo samples. Their resolution was such that they identified most levels below ~500-eV energy, but missed, or failed to resolve, multiple structure for many "levels" above ~1 keV. The isotope assignments for the levels shown in Table I are on the basis of their measurements where we were reasonably assured that the particular level energy and $ag\Gamma_n^0$ that we obtained correlated with one of their assignments. Higher resolution measurements using separated isotopes would be helpful in clarifying the assignments.

When our level energies and $ag\Gamma_n^0$ values for natural Mo are compared with those of Pevsner *et al.*[4] and earlier measurements,[3] the agreement is fairly good in most cases when the poorer energy resolution of the earlier work is considered. Pevsner *et al.* obtain values of Γ_γ for a few resonances of most isotopes from capture γ-ray studies. Their results give $\Gamma_\gamma\sim200$–300 meV for all isotopes. Recently Kim *et al.*[6] have presented results for Γ_γ for five levels of the Mo isotopes $A=95$, 96, 97, 98. They list Γ_γ values from 175–210 meV, with quoted uncertainties of ~30 meV.

The most relevant previous studies for Sb are those of Palmer and Bollinger,[7] and Jackson and Bollinger,[8] which provide the isotope assignments for the levels in Tables II and III for which such assignments are given. Palmer and Bollinger used samples of normal Sb and of Sb^{123} and made total-cross-section measurements using the Argonne fast chopper with a highest resolution of 120 nsec/m. Their energy resolution was not sufficient to resolve all level structure above 75–100 eV.

The isotope assignments for more resonances to 233.6 eV were made by Jackson and Bollinger using natural Sb samples on the basis of the shape of the γ-ray capture spectra for the different resonances. The isotope identifications in Tables II and III are based on their results. It would be desirable to extend the range of isotope identification by high resolution studies using separated Sb isotopes.

Stolovy and Harvey[9] and Bolotin and Chrien[10] have obtained both Γ_γ and $g\Gamma_n^0$ values for a few of the lowest-

[6] Kim Hi San, L. B. Pikel'ner, Kh. Sirazhet, and E. I. Sharapov, Zh. Eksperim. i Teor. Fiz. **49**, 410 (1965) [English transl.: Soviet Phys.—JETP **22**, 288 (1966)].

[7] R. R. Palmer and L. M. Bollinger, Phys. Rev., **102**, 228 (1956).

[8] H. E. Jackson and L. M. Bollinger, Phys. Rev., **124**, 1142 (1961).

[9] A. Stolovy and J. A. Harvey, Phys. Rev., **108**, 353 (1957).

[10] H. H. Bolotin and R. E. Chrien, Nucl. Phys. **42**, 676 (1963).

TABLE IX. Favored spin values for some resonances in Pr. The headings S, D, and C, respectively, denote assignments by groups at Saclay (Julien *et al.*),[a] Dubna (Wang *et al.*),[b] and Columbia University (the present work). Levels marked with an asterisk are prominent resonances for which one or more groups favor a spin value of $J=2$. The three groups have generally good agreement on the $g\Gamma_n^0$ values for the levels. The tabulated values here are "weighted averages" of $g\Gamma_n^0$ for the different groups. Values of J shown in parentheses represent more uncertain assignments.

E_0 (eV)	Favored J values S	C	D	$g\Gamma_n^0$ (meV)
218.65	3	3	3	90
235.20	3	2	(3)	66*
359.7	2	3	3	75*
387.9	3	···	···	3
519.6	2	2	3	38*
635.4	3	3	···	120
721.0	2	2	···	90*
845.2	3	3	3	190
957.2	2	2	2	105*
1120.0	3	···	···	40
1484.0	3	2	···	130*
1715.5	3	3	···	80
1880	···	(2)	···	4
2096	3	3	···	165
2132	3	···	···	23
2452	3	3	···	35
2926	···	3	···	10
2998	3	3	···	240
3156	···	2	···	10.5
3474	···	(3)	···	15
3603	2	(3)	···	130*
3780	3	(3)	···	145
3928	···	(2)	···	27
4002	···	(2)	···	7
4544	3	···	···	80
4587	2	···	···	83*
5250	3	···	···	47
5600	2	···	···	150*
5734	3	···	···	44

[a] Reference 3. [b] Reference 14.

energy resonances. Table VIII compares our results with those of the other groups for some levels in Sb below 100 eV. The $2g\Gamma_n^0$ values of Palmer and Bollinger are for $\Gamma_\gamma=100$ meV (assumed). The mean Γ_γ value seems to be ~100 meV. The range of values obtained by the different groups for each level is about as large as the variation from level to level.

Assignments of resonances in natural Te to individual isotopes in Table IV are made on the basis of assignments using separated isotopes by Danelyan *et al.*[11] Cote[12] has also made isotope assignments, mainly on the basis of the resonance capture γ-ray spectra shape. Bilpuch *et al.*[13] have measured the energies and Γ_n values for 21 levels in Te^{130} from 1.5–117.5 keV. Our resonance at 1557 eV may correspond to their level at 1.5±0.5 keV on the basis of its large $ag\Gamma_n^0$ value, but the strong levels at 1839 and 1933 eV could also be the level observed by Bilpuch. The next level in Te^{130} is at 10 keV.

Our $ag\Gamma_n^0$ values for Te are generally in fair agreement with those of other groups where comparisons[3] can be made. The Γ_γ values obtained by other groups are ~100 meV for the Te isotopes.

We have already mentioned the encouraging satisfactory agreement of our level energies and $g\Gamma_n^0$ for Pr with those of Julien *et al.*[3] They employed a more sophisticated shape analysis for their resonance analysis which gives extra information useful for determining J values and Γ_γ in favorable cases. Wang *et al.*[14] have also determined values of $ag\Gamma_n^0$, Γ_γ, and J for some of the lower-energy resonances. All values except our final results are tabulated in Ref. 3. A comparison of results for applicable levels is given in Table IX. Of the six cases where all three groups obtained favored J values, all agree in three cases. Of the nine cases where only Saclay and Columbia values are given, we agree in seven cases.

The determinations of Γ_γ for Pr which have been made since 1963 by the various laboratories are mainly in the range from 70–110 meV. We have made use of this in our analysis of the Pr data as indicated in the discussion of Figs. 5(c) and (d).

C. Distribution of $ag\Gamma_n^0$ Values

Natural Mo and Te have far too many isotopes of widely varying abundance and level spacing to render meaningful a detailed test of the distribution of $ag\Gamma_n^0$ against, for example, the Porter-Thomas theoretical distribution. We noted in discussing Figs. 7(a) and 7(c) that a few of the levels were abnormally strong in terms of what is expected for a single Porter-Thomas[15] population.

In the case of natural Sb, the four (spin-isotope) compound-nucleus populations for $l=0$ have not too unequal representation, and not too dissimilar $\langle ag\Gamma_n^0\rangle$ values are expected. It is, therefore, not unreasonable to think that a single-population Porter-Thomas distribution might give a fair fit. Figure 8 shows a histogram plot of the relative number of levels having $(ag\Gamma_n^0)^{1/2}$ values in successive 0.1-$meV^{1/2}$ steps for levels in the energy range to 1.2 keV. The Porter-Thomas function ($\nu=1$) would be a Gaussian peaked at $y\equiv(ag\Gamma_n^0)^{1/2}=0$. For a two-channel ($\nu=2$) distribution, the expected curve is of the form $x\exp(-x^2/2)$, where x is proportional to $(ag\Gamma_n^0)^{1/2}$ and a suitable normalization is used. The $\nu=2$ distribution discriminates against very small values of y, while the experimental histogram of Fig. 8 clearly has a large excess in the first box which prevents a good fit with $\nu=1$.

One can argue that the interval $y=0$–0.1 should probably *not* be trusted as being correct for the $l=0$

[11] L. S. Danelyan and B. V. Efimov, Soviet J. At. Energy **14**, 258 (1964).
[12] R. E. Cote (private communication).
[13] E. G. Bilpuch, K. K. Seth, C. D. Bowman, R. H. Tabony, R. C. Smith, and H. W. Newsom, Ann. Phys. (N. Y.) **14**, 387 (1961).
[14] Wang Nai Yen, N. Iliescu, E. N. Karzhavina, Kim Hi San, A. B. Popov, L. B. Pikel'ner, T. Stradnikov, E. I. Scharapov, and Yu. S. Yazvitskii, Zh. Eksperim. i Teor. Fiz. **47**, 43 (1964) [English transl.: Soviet Phys.—JETP, **20**, 30 (1965)].
[15] C. E. Porter and R. E. Thomas, Phys. Rev. **104**, 483 (1956).

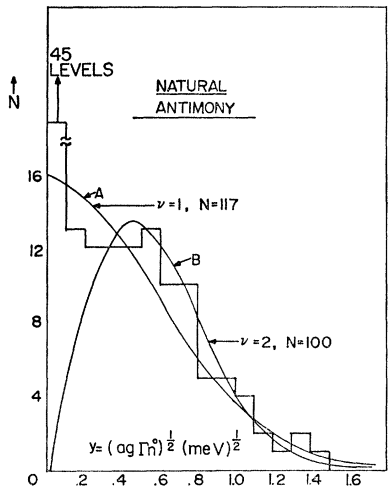

FIG. 8. A histogram for the observed distribution of $(ag\Gamma_n^0)^{1/2}$ values in natural Sb for neutron resonances below 1200-eV neutron energy. The excess of weak levels is attributed to $l=1$ resonances. One- and two-channel Porter-Thomas theoretical curves are compared with the experimental results as discussed in the text. The curves are normalized to the indicated number of levels.

population because this is just where the $l=1$ population should appear. If one tries for a best fit of the *rest* of the histogram to a Porter-Thomas ($\nu=1$) distribution, the excess of observed cases will be attributed to (a) observed $l=1$ levels, plus (b) spurious "noise" levels, minus (c) missed weak $l=0$ levels. Curve A in Fig. 8 is normalized assuming that 30 of the 45 levels in the first box are not $l=0$. The remaining defining condition is to require that it have the same $\sum ag\Gamma_n^0$ as the experimental distribution. The fit to all but the first interval is seen to be quite satisfactory.

If one seriously believed that a $\nu=2$ theoretical curve should fit, the obvious excess in the first two histogram boxes would suggest that one should assume that both of these boxes are "contaminated" with $l=1$ levels and confine attention to a fit to the rest of the histogram. In this case a total of about 47 levels would be deducted from the first two boxes. Curve B is normalized to 100 levels and is also adjusted to the observed $\sum ag\Gamma_n^0$. It is seen that this gives a quite acceptable fit to all but the first two boxes. However, we do not believe that $\nu=2$ is a reasonable choice to represent the physics of the process. Our interpretation is based on the above discussion in terms of the Porter-Thomas distribution, as modified by considerations resulting later from an inspection of the nearest spacing distribution.

Figure 9 shows the corresponding distribution for Pr for the entire energy ranges 0–5 keV and 5–10 keV. The range 0–10 keV gave a linear plot of number of observed levels versus energy. It is obvious that the histograms are poorly suited for fitting with either a $\nu=1$ (Porter-Thomas) or $\nu=2$ theoretical shape. The histogram uses $\Delta y=2$ meV$^{1/2}$ steps and coincides exactly for the first two steps for the two energy regions. The upper energy region has fewer relative strong levels than the first. This was also clear from Fig. 7(d). The histogram for the 0–5-keV region is probably more significant than for the higher energies.

One expects $\langle g\Gamma_n^0\rangle \sim 0.1$ meV for $l=1$ levels which are analyzed as $l=0$ levels in this energy region, assuming an "average" $l=1$ strength function. A reference to Table V shows that only a relatively small number of "levels" were assigned values of $g\Gamma_n^0 \lesssim 0.1$ meV, so it is difficult to understand Fig. 9 on the basis of an appreciable $l=1$ contribution. This is particularly true for the second box of the histogram.

There is a temptation to view the observed histogram as due to the sum of two Porter-Thomas distributions, one accounting for the stronger levels and having a height of ~ 6 at the first box. The second distribution would need to have a height ~ 20 at the first box and fall to a relatively small value at the third box. Each distribution would account for approximately half the levels.

The interpretation for Pr of two widely different $\langle g\Gamma_n^0\rangle$ populations requires further consideration since there is only one isotope, and the compound-nucleus spin values $J=2$ and 3 are of comparable size. An obvious basis for a population division lies in the values of J for the resonance. One notes that Pr has a relatively large value for S_0 compared with the preceding neighboring nuclei to $A\sim 90$. A reference to Seth's review[5] of S_0 values for all nuclei shows that the first "large" S_0 value (1.8 ± 0.6) in this region is for $_{56}Ba^{138}$ which also has $N=82$. However, $_{57}La^{139}$ seems to have a significantly smaller S_0 on the basis of a preliminary analysis of our results for La, and from other reported[5] values. For these $N=82$ nuclei the initial nucleus plus neutron entrance channel has all neutrons except the incident neutron in the closed $N=82$ configuration. A strong single-particle excitation doorway state may be involved for the population with large $\langle g\Gamma_n^0\rangle$, but not for the other. The simplest interpretation for two such different populations would have one population corre-

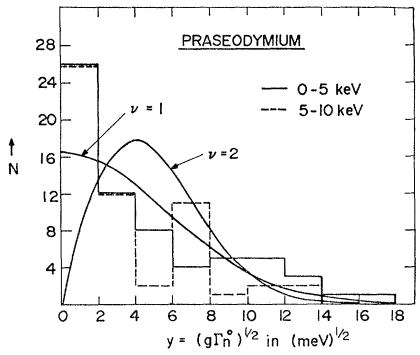

FIG. 9. Histogram of the observed distributions of $(g\Gamma_n^0)^{1/2}$ values for Pr for neutron resonances between 0–5 and 5–10 keV. The $\nu=1$ and $\nu=2$ theoretical curves are normalized to the observed number of levels for 0–5 keV.

spond to $J=3$ and the other to $J=2$. If this interpretation proves to be unacceptable, a "hidden quantum number" could be considered as being present which involves other symmetry aspects of the doorway state. The Porter-Thomas distribution is only expected to apply in the absence of such "hidden-partly good" quantum numbers.

Table IX lists the levels in Pr for which we, the Saclay,[3] or Dubna[14] groups list favored J values, along with the quoted[3] J values and a "compromise" value for $g\Gamma_n^0$. It is clear that $J=3$ would be favored for the population having large $\langle g\Gamma_n^0\rangle$ values. The test then is to see if one can reconcile the $J=2$ case with the smaller $\langle g\Gamma_n^0\rangle$ distribution which should have very few cases with $g\Gamma_n^0 \gtrsim 25$ meV from the above reasoning. Asterisks are placed after the $g\Gamma_n^0$ values which should be $J=3$ by this reasoning, but for which one or more groups favored $J=2$. It is difficult to exclude $J=2$ for all of these strong levels. The situation probably warrants further future investigation.

D. Level-Spacing Distributions and Other Statistical Tests

A study of the nearest-neighbor level-spacing distribution, and a comparison of results for successive energy intervals, provides a sensitive indication of the extent to which the decreasing energy resolution at higher energies causes one to miss an increasing fraction of the small level spacings. Figure 10 shows the experimental histograms for the observed number of nearest-neighbor level spacings in successive 3-eV intervals for natural Sb for the energy intervals 0–600 eV and 600–1200 eV. Figure 11 shows the histograms for Pr in 30-eV spacing intervals for the full 0–10-keV energy interval, and the separate contributions from the 0–5-keV and 5–10-keV energy intervals. For both elements it is evident that there are relatively few spacings in the first histogram box for the upper

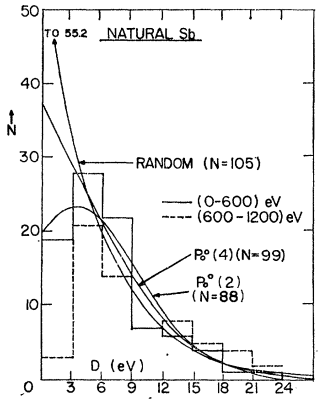

FIG. 10. Histograms of the observed distributions of nearest-neighbor level spacings for natural Sb for $E_n=0$–600 eV and 600–1200 eV. The experimental results are compared with theoretical curves as shown.

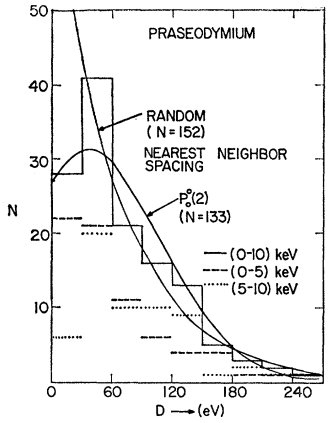

FIG. 11. Histogram of the observed distributions of nearest-neighbor level spacings in Pr for $E_n=0$–10 keV. The separate contributions of the energy regions 0–5 keV and 5–10 keV are also shown. Comparison is made with theoretical curves as shown.

energy region compared with the number for the second energy region. A missed small spacing corresponds experimentally to a situation where two levels count as one or a weak level is missed. One of the larger observed spacings should be broken up into two (or more) smaller spacings in such cases. The 395-eV spacing between the "adjacent" nearest-neighbor levels at 4002 and 4397 eV in Pr is much too large to be allowed by any present theory. It probably reflects missing weak levels between the two observed levels, so this spacing would be expected to break into two (or more) smaller spacings.

For a single (spin-isotope)-level population we now believe that the Wigner level repulsion theory should apply. This has been discussed in more detail in earlier papers[1] of this series which contain references to the extensive theoretical literature. The orthogonal (Wigner) distribution, denoted $P_0^0(1)$, is of the functional form $x\exp(-x^2/2)$, where x is proportional to the spacing D and is normalized to yield the proper $\langle D\rangle$. For natural Sb there are four (spin-isotope) populations for $l=0$ while there are two for Pr. One usually assumes that these are distinct noninteracting populations (ensembles), randomly positioned relative to each other. One can readily calculate the expected nearest-neighbor level spacing distribution when n independent populations, having known spacing distributions $P_j(s)$ are randomly positioned with respect to each other. As $n\rightarrow\infty$ one approaches a random, e^{-x}-type resultant distribution.

The theoretical curves in Figs. 10 and 11 show the expected spacing distribution shapes for the cases of two and four superimposed equal-level density populations each having a Wigner spacing distribution. A comparison with experiment is complicated by (a) the partial presence of an $l=1$ population for Sb, with decreasing probability of detecting $l=1$ levels with increasing neutron energy; (b) the fact that the different spin-isotope populations for natural Sb and for

Pr probably do not have equal level densities; and (c) the experimental missing of many small spacings. The effect (b) should be similar to decreasing n, while (a) should be similar to increasing n. The probability of observing small level spacings, in units of the mean level spacing, should increase as the effective n increases. Thus (a) above could account for a small part of the larger number of small spacings observed in the lower relative to the higher-energy region for natural Sb. Effect (c) suggests that one should *not* necessarily normalize the theoretical curves in Figs. 10 and 11 to the observed number of spacings. The theoretical curves have been normalized to give an optimum fit to all of the histogram except for the first box. Increasing the assumed number of spacings N in a given energy interval stretches the theoretical curve vertically, and shrinks it horizontally in a way that keeps the area under the curve equal to $N\Delta D$, and the first moment equal to $N\Delta E\Delta D$, where ΔE=energy interval and ΔD=histogram box width. In Fig. 10 for a 600-eV energy region in natural Sb, we obtain 88 spacings in the first 600-eV region and 64 in the second. The random distribution curve is normalized to 105 spacings, the $P_0^0(2)$ two-population curve is normalized to 88 spacings, and the $P_0^0(4)$ curve is normalized to 99 spacings. The corresponding implied $\langle D\rangle$ values are 5.7, 6.8, and 6.0 eV, respectively.

In Fig. 11 for Pr we normalize the theoretical curves to 152 spacings (for 10 keV) for the random, $\langle D\rangle=66$ eV, and to 133 spacings for $P_0^0(2)$, $\langle D\rangle=75$ eV. In comparing the theoretical distribution curves with the experimental histograms, one should visualize the result if the implied number of observed spacing values are each split into two smaller spacings. The four- and two-population theoretical curves are *a priori* expected to yield the best fits for natural Sb and Pr, respectively.

E. Further Analysis

In previous papers[1] we determine correlation coefficients between various parameters for each element and presented distribution curves for higher-order level spacings. These tests are of interest where one or more statistical populations are fully represented without excess contamination by false levels, or an incompletely detected population component.

The same further analyses were made for the results on the elements presented in this paper. In accordance with the preceding discussion of the paper we do not believe that these tests are sufficiently meaningful and may be misleading, for our results on Mo, Sb, Te, and Pr to warrant presentation.

ACKNOWLEDGMENTS

The authors take pleasure in acknowledging the assistance of H. I. Liou and the velocity selector technicians, A. W. Blake, D. Ryan, and J. Spiteri, in the various phases of these measurements. B. E. Ham gave much assistance in the programming used for data reduction and J. Cleary helped greatly with the careful preparation of the figures. Finally we wish to express our appreciation of the assistance rendered by the technical staff of the Nevis synchrocyclotron.

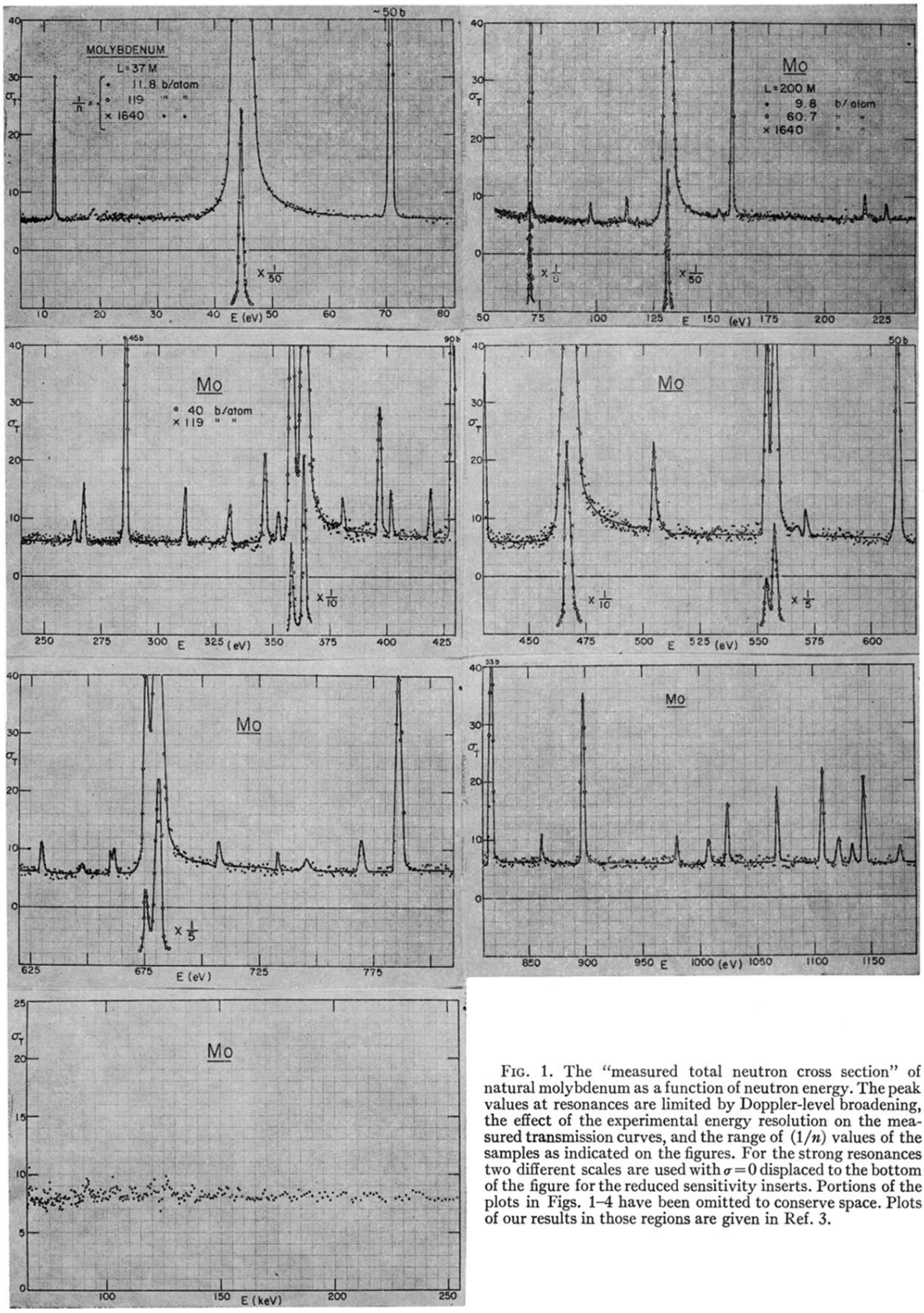

FIG. 1. The "measured total neutron cross section" of natural molybdenum as a function of neutron energy. The peak values at resonances are limited by Doppler-level broadening, the effect of the experimental energy resolution on the measured transmission curves, and the range of $(1/n)$ values of the samples as indicated on the figures. For the strong resonances two different scales are used with $\sigma=0$ displaced to the bottom of the figure for the reduced sensitivity inserts. Portions of the plots in Figs. 1–4 have been omitted to conserve space. Plots of our results in those regions are given in Ref. 3.

FIG. 2. The "measured" σ_T-versus-E_n curves for natural antimony. The text and the caption for Fig. 1 give a detailed explanation.

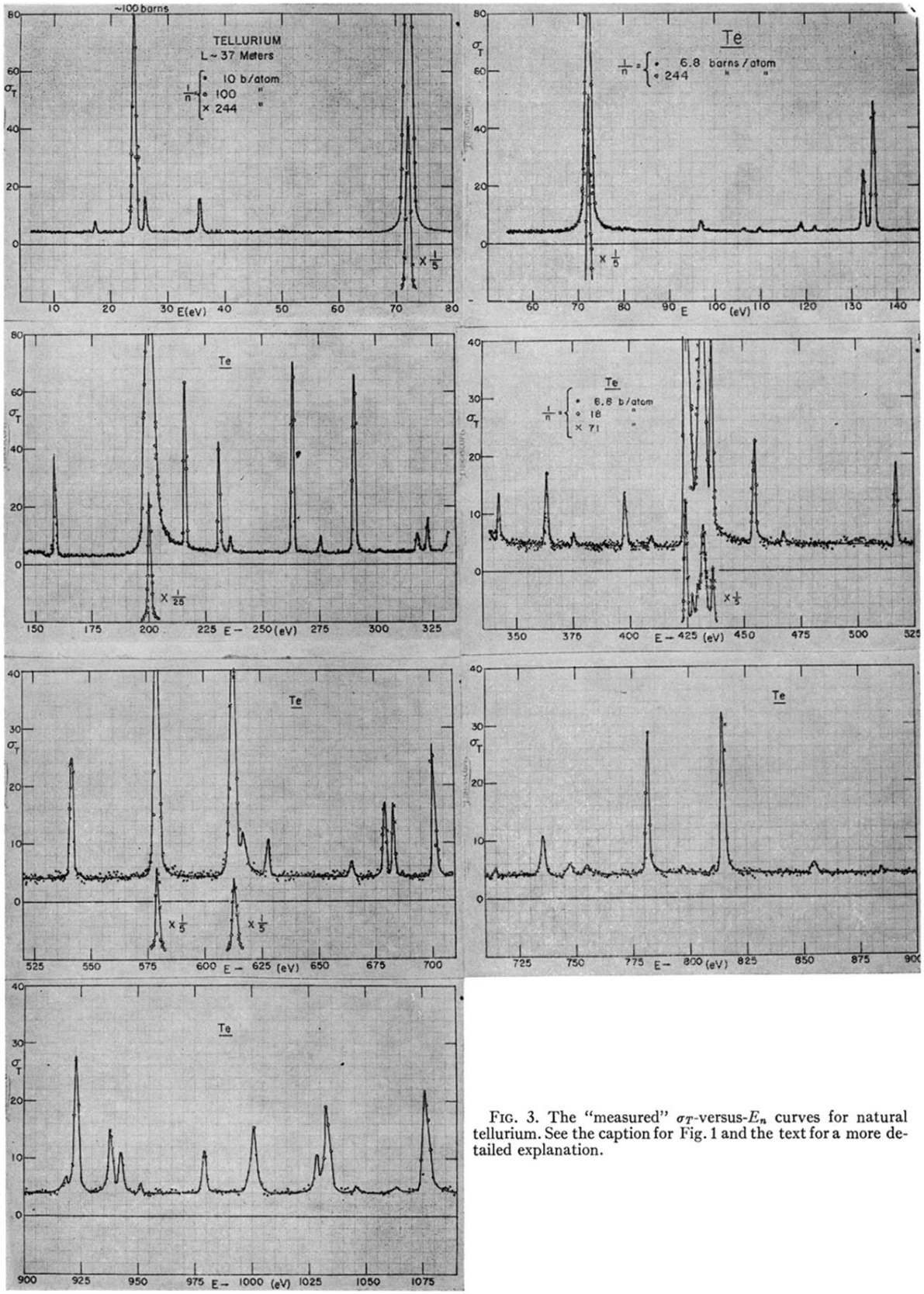

FIG. 3. The "measured" σ_T-versus-E_n curves for natural tellurium. See the caption for Fig. 1 and the text for a more detailed explanation.

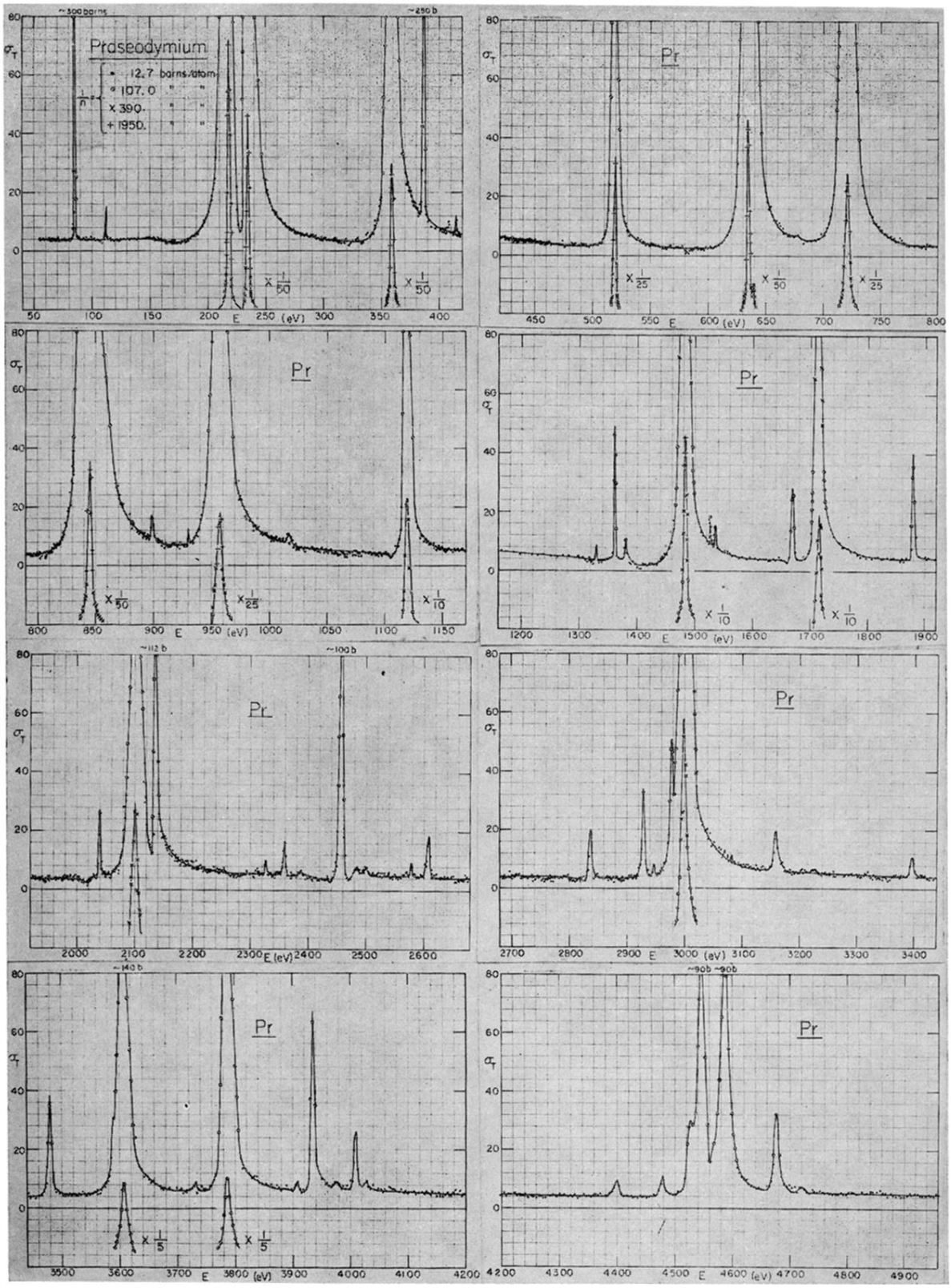

FIG. 4. The "measured" σ_T-versus-E_n curves for praseodymium. See the text and the caption for Fig. 1 for a detailed explanation.

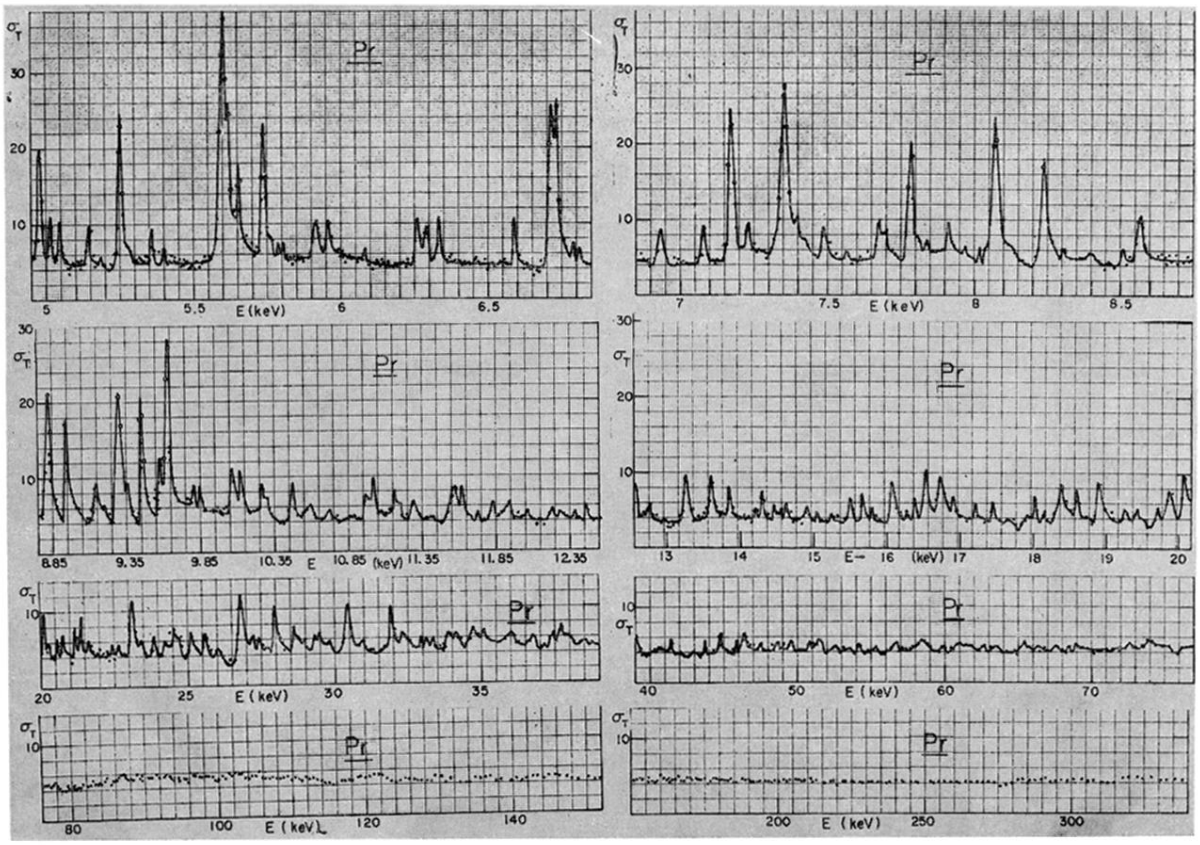

FIG. 4 (*continued*)